Archaeological and Anthropological Sciences

The ancient pozzolanic mortars and concretes of Heliocaminus baths in Hadrian's Villa (Tivoli, Italy)

--Manuscript Draft--

Manuscript Number:	
Full Title:	The ancient pozzolanic mortars and concretes of Heliocaminus baths in Hadrian's Villa (Tivoli, Italy)
Article Type:	Special Issue on Provenance, technology and dating issues in Archaeometry
Section/Category:	Provenance, technology and dating issues in Archaeometry
Corresponding Author:	Stefano Columbu, MD Universita degli Studi Di Cagliari Cagliari, CA ITALY
Corresponding Author Secondary Information:	
Corresponding Author's Institution:	Universita degli Studi Di Cagliari
Corresponding Author's Secondary Institution:	
First Author:	Stefano Columbu, MD
First Author Secondary Information:	
Order of Authors:	Stefano Columbu, MD
	Fabio Sitzia, MD
	Guido Ennas
Order of Authors Secondary Information:	
Funding Information:	
Abstract:	Aim of this work is the Baths with Heliocaminus, a special and unique architectural building in the complex of the Hadrian's Villa in Tivoli. This research is carried out with a multidisciplinary approach combining physical-mechanical to petrographic-mineralogical characterization. 30 samples were investigated for composition and physical properties (density, porosity, water absorption, mechanical strength, particle-size distribution of aggregate, etc.), representative of eight mortar groups: cubilia mortar, brick bedding mortars, floor-coating and wall-coating bedding mortars, floor (rudus) and wall conglomerates (trullisatio), vault concretes, plasters (arriccio). Physical parameters, together microscopic analysis and binder/aggregate ratio determined in three ways using image analysis (on thin sections and on specimens) and weight-data from dissolution of binder, have shown interesting relationship between the physical and compositional characteristics and the function of mortars within the structure of the Heliocaminus baths. To identification the primary compounds, the reaction phases between binder and aggregate and hydraulic degree, the samples were analysed also with XRD methodology, thermo-gravimetry (TGA) and differential scanning calorimetry (DSC). The results highlight a correlation between the pozzolanic characteristics and physical-mechanical properties of the mortars (i.e., punching strength index).
Suggested Reviewers:	Dagmara Wielgosz-Rondolino University of Warsaw dagmara.wielgosz@uw.edu.pl - archaeology issue
	Marco Giamello Universita degli Studi di Siena marco.giamello@unisi.it - petroarchaeometry on cultural heritage - geoarchaeology

	- provenance of raw materials

The ancient pozzolanic mortars and concretes of Heliocaminus baths in Hadrian's Villa (Tivoli, Italy)

***Stefano Columbu[a], Fabio Sitzia[a] , Guido Ennas[b]**

* Corresponding author - *columbus@unica.it*

[a] *Department of Chemical and Geological Sciences, University of Cagliari – Via Trentino 51, 09127 Cagliari (Italy) – Tel.+39-070-6757766, Fax +39-070-282236 - columbus@unica.it*

[b] *Department of Chemical and Geological Sciences, University of Cagliari – Cittadella Universitaria di Monserrato, 09042 Monserrato (Italy) –Tel +39-070-6754364, Fax +39-070-6754388 - ennas@unica.it*

Abstract:

Aim of this work is the Baths with *Heliocaminus*, a special and unique architectural building in the complex of the Hadrian's Villa in Tivoli. This research is carried out with a multidisciplinary approach combining physical-mechanical to petrographic-mineralogical characterization. 30 samples were investigated for composition and physical properties (density, porosity, water absorption, mechanical strength, particle-size distribution of aggregate, etc.), representative of eight mortar groups: *cubilia* mortar, brick bedding mortars, floor-coating and wall-coating bedding mortars, floor *(rudus) and* wall conglomerates *(trullisatio)*, vault concretes, plasters *(arriccio)*.

Physical parameters, together microscopic analysis and binder/aggregate ratio determined in three ways using image analysis (on thin sections and on specimens) and weight-data from dissolution of binder, have shown interesting relationship between the physical and compositional characteristics and the function of mortars within the structure of the *Heliocaminus* baths.

To identification the primary compounds, the reaction phases between binder and aggregate and hydraulic degree, the samples were analysed also with XRD methodology, thermo-gravimetry (TGA) and differential scanning calorimetry (DSC). The results highlight a correlation between the pozzolanic characteristics and physical-mechanical properties of the mortars (i.e., punching strength index).

Keywords: Hadrian's Villa, Binder, Aggregate, Thermal Analysis, XRD Analysis Pozzolanic, Ancient mortars.

1. Introduction

Built close to the area of the Republican residence of the Emperor from the year 118 A.D. (Fig. 1), the baths with *Heliocaminus* (Figs. 1, 2) are the oldest spa building of Hadrian's Villa. Its name derives from the identification of the imposing circular room with *Heliocaminus*, a particularly warm environment, as well as from sunlight, even from a traditional system with hypocaust (Mac Donald and Pinto 2006). Recently, this room has been recognized as a *sudatio*, for the presence of bakery openings that could supplement the warm derive from the floor and the wall necessary for the sauna (Salza Prina Ricotti 2000). The hall, covered by a coffered dome with central eye, was equipped with large windows, now fully collapsed, facing to the south-western side, where are located all the heated rooms of Villa Adriana. This orientation reflects faithfully the requirements dictated by architect Vitruvio (Pollione 15 BC; Verduchi 1975; Cicerchia 1985; Giuliani Cairoli 2006). The building with *Heliocaminus* presents innovative architectural features that were given by the same Emperor Hadrian (Mac Donald and Pinto 2006). The construction materials such as marble coating (Attanasio et al. 2009, 2013; Columbu et al. 2014a; Lapuente et al. 2012; Pensabene et al. 2012), the stone filling of the curtain walls and the not decorated mosaic in the corridors of floors are rather similar to those used in other buildings of the Villa and confirms the relevance of the complex to the noble zone (Cagnana 2000; Adam 2006).

For laying all several kind of construction materials several type of aerial and hydraulic mortars were used in Hadrian's Villa for bedding bricks, *cubilia* small ashlars, marble slabs and plaster (Fig. 2). The mortars present a variable composition and hydraulic degree according to their function in building: e.g., for improve the physical-mechanical strength (i.e., wall structure, foundations, raised floors, etc.) or as waterproofing (i.e., cisterns, etc.). For these reasons, their use was especially done in medium or high humidity environments such as Roman baths. In hydraulic mortars the degree of pozzolanicity is conferred by the chemical reaction between glassy acid volcanic aggregates (e.g., pyroclastites) or by articial pozzolans (i.e., cocciopesto).

The compositional characteristics of the mortars are fundamental to define the construction phases of ancient building and to trace the technologies used in the historical periods (Miriello et al. 2010a, 2010b, 2015; Columbu et al. 2015; Crisci et al. 2001, 2002; De Luca et al., 2013; Maravelaki-Kalaitzaki et al. 2003; Moropoulou et al. 1995, 1999, 2000, 2002, 2003a, 2003b, 2004; Paama et al. 1998; Palomo et al. 2002; Riccardi et al. 1998; Smith and Smith 2009; Vola et al. 2011), especially when in combination with 3D laser-scan relief methods of the monument structures (Columbu and Verdiani 2011, 2014; Verdiani and Columbu 2010; Lezzerini et al. 2016).

Also the physical properties (porosity, bulk density, mechanical strength, etc.) are significant for study the alteration processes (Columbu et al. 2014b) and consequently to address the conservation and restoration interventions (Callebaut et al. 2001; Moropoulou et al. 2013).

The following paper is a work started by Columbu et al. (2015). It proposes the study of the bedding mortars, *cocciopesto*-conglomerates and concretes from *Heliocaminus* Baths through an archaeometric multidisciplinary approach characterized by mineralogical-petrographic-physical-mechanical analysis, including particle size of the aggregate. 30 samples from main sectors of the theater (i.e., tribunalia vaults, cavea tiers, stage walls, vaults, brick walls of external niches, structure masonry) were analysed.

The analysis are addressed to define the mixture technologies of raw material according to ancient Roman mode and uses (Miriello et al. 2010; Miriello et al. 2011; Bultrini et al. 2006; Fly et al. 2011; Stanislao et al. 2011; Adriano et al. 2009).

By polarizing microscope analysis the mineralogical composition and petrographic characteristics of mortars were determined. The petrographic study, together image analysis on thin sections and on bulk mortar specimen faces, can provide significant data about: a) preparation of mortars and different mixing ratios of binder and aggregate; b) geological origin of raw materials used as aggregate (*e.g.*, volcanic scoria, leucitites); c) selection method of raw materials in relation to the function of mortar in the building.

Then, to define the hydraulic degree of mortars, thermo-gravimetric and differential scanning calorimetry analysis (TG and DSC) together XRD analysis were also made on enriched powered of binder, according to well-known experimental methods (Bultrini et al. 2006; Drdácky et al. 2013; Ricciardi et al. 1998; Maravelaki-Kalaitzaki et al 2003; Miriello et al. 2010; Miriello et al. 2011; Moropoulou et al. 2003a; Moropoulou et al. 2003b; Moropoulou et al. 1999; Maravelaki-Kalaitzaki et al., 2004; Babini and Fiori 1996; Bakolas et al. 1998; Topçu and Isıkdag 2012; Bultrini et al. 2006; Moropoulou et al. 1995; Ortega et al. 2008; Palomo et al. 2011). Analytical data were compared to the physical-mechanical properties (i.e., point load strength) for define their relationship (Topçu and Isıkdag 2012; Papayianni et al. 2013).

Furthermore, the analysis of other physical properties (water absorption and saturation) allows us to verify the building and production quality of mortars.

2. Materials and methods

2.1 Materials

30 samples collected from the *Heliocaminus* Baths of mortars were analysed (Fig. 3). The samples are representative of mortars with different functions in the baths (according to 8 groups, Columbu et al. 2015), such as: 7 brick bedding mortars (*Opus Testaceum*), 3 *Cubilia* bedding mortars (*Opus Reticolatum*), 4 floor-coating bedding mortars (*Marmor pavimentum*), 3 wall-coating bedding mortars (*Harenata marmor*), 5 floors conglomerates with (*Opus Signinum* of *Rudus*), 3 wall conglomerates (*Opus Signinum* of *Trussillatio* or *rinzaffo* layers), 3 concretes of collapsed vaults (*Opus Caementitium*), and 2 plasters (*arriccio* layers).

4 lime lumps of mortars were also analysed to understand their composition and modality of formation. The mortars with the same function were sampled according to different heights in the structure and/or in diverse environments.

Samples of mortars and stones regard the superficial portions of material, having maximum volumes of about 25 cm^3, compatibly with the limits imposed by the Superintendence of Cultural Heritage of Lazio Region, which has imposed a maximum number and quantity of samples. However, the size of the material taken from the baths is representative and suitable for determine the compositional and physical characteristics of the mortars studied.

The mortars with the same function are related to different sampling heights in the structure and/or in diverse room of baths.

2.2 Analytical methods

Petrographic determinations of mineralogical composition were carried out by optical polarised microscopy on polished thin sections on 38 samples (30 of consolidated by epoxy resin mortars, 3 *lateritious*, 5 volcanics). Modal analysis of mortars has been determined with "points counter" on about 300 points for each thin section.

The binder/aggregate ratio (B/A) of mortars was calculated through image analysis (by ImageJ 1.47v) in two different ways: i) on photographs taken on 6 faces of the cubic specimens of mortars on which the physical-mechanical tests have been determined; ii) on thin section photographs detected with the flatbed scanner. The binder/aggregate ratio (B/A) was calculated also with weight data from acid dissolution of mortar binder for determine the particle size of aggregate (see text and figure captions of manuscript).

A Seifert X3000 apparatus in the Bragg–Brentano geometry was used for X-Ray Powder Diffraction. It was operated using the CuKa radiation in the range of 8–40 (2J degrees) with step of 0.05 2□, with an opportune counting time to optimize the signal/noise ratio. JCPDF-2 database1 was used for the identification of the phases.

Regarding the thermo-gravimetric analysis, two grams of each mortar (without the coarse aggregate) were ground by Giuliani IG colloidal mill. W2/E/S. to enrich the sample in the binder fraction, the powder was treated with Frantz magnetic separator for the removal of the iron-magnetic mineral fraction present in the sample. The analysis (TGA) measurements were carried out at atmospheric pressure using a Perkin Elmer instrument model TGA7. The measurements were performed under Ar flow (60 mL min-1). Samples of 10 mg were placed in platinum crucibles and scanned in the temperature range of 30–900 °C with a heating rate of 10 °C min-1. The calorimeter was calibrated by measuring the melting temperature of metallic Indium and Zinc (99.999 mass% purity) and the temperature was obtained with an accuracy of ± 0.5 °C.

The physical tests were determined on 82 cubic specimens (with an average size of 15•15•15 mm) extracted from unaltered portion of samples after removing the exterior part of mortar. The physical properties analysis was made also on small fragment (only for some mortar samples) of volcanic and cocciopesto aggregates extracted from mortars.

The specimens were dried at 105 ± 5°C and the dry solid mass (m_D) was determined. The solid phases volume (V_S) of powdered rock specimens (on 5-8 g and with particle size less than 0.063 mm) and the real volume (with $V_R = V_S + V_C$, where V_C is the volume of pores closed to helium) of the specimens were determined by helium Ultrapycnometer 1000 (Quantachrome Instruments).

Then, the wet solid mass (m_W) of the samples was determined after water absorption by immersion for ten days. Through a hydrostatic analytical balance, the bulk volume V_B (with $V_B = V_S + V_O + V_C$, where $V_O = (V_B-V_R)$ is the volume of open pores to helium) is calculated as:

$$V_B = [(m_W-m_{HY})/\rho_w T_{25°C}]\cdot 100$$

where m_{HY} is the hydrostatic mass of the wet specimen and $\rho_W T_{25°C}$ is the water density at a temperature of 25°C.

Total porosity (Φ_T), open porosity to water and helium ($\Phi_O H_2O$; $\Phi_O He$, respectively), closed porosity to water and helium ($\Phi_C H_2O$; $\Phi_C He$), bulk density (ρ_B), real density (ρ_R), solid density (ρ_S) were computed as:

$$\Phi_T = [(V_B-V_S)/V_B]\cdot 100$$

$$\Phi_O H_2O = \{[(m_W-m_D)/\rho_W T_X]/V_B\}\cdot 100$$

$$\Phi_O He = [(V_B-V_R)/V_B]\cdot 100$$

$$\Phi_C H_2O = \Phi_T - \Phi_O H_2O$$

$$\Phi_C He = \Phi_T - \Phi_O He$$

$$\rho_S = m_D/V_S\ ;\ \rho_R = m_D/V_R\ ;\ \rho_B = m_D/V_B$$

The weight imbibition coefficient (IC_W) and the saturation index (SI) were computed as:

$$IC_W = [(m_W-m_D)/m_D]\cdot 100$$

$$SI = (\Phi_O H_2O/\Phi_O He) = \{[(m_W-m_D)/\rho_W T_X]/V_O\}\cdot 100$$

The punching strength index was determined with a Point Load Tester (mod. D550 Controls Instrument) according with the ISRM (1972, 1985) on the same pseudo-cubic rock specimens used for other physical properties. The load was exerted via the application of a concentrated load with two opposing conical punches.

The resistance to puncturing (I_S) was calculated as P/D_e^2, where P is the breaking load and D_e is the "equivalent diameter of the carrot" (ISRM, 1985), with $D_e = 4A/\pi$ and $A = W\cdot D$, where W and 2L are the width perpendicular to the direction of the load and the length of the specimen, respectively. The index value is referred to a standard cylindrical specimen with diameter D = 50 mm for which I_S has been corrected with a shape coefficient (F) and calculated as:

$$I_{S(50)} = I_S\cdot F = I_S\cdot(D_e/50)^{0.45}$$

The simple compression resistance (R_C) and the traction resistance (R_T) of the mortar were indirectly calculated (according to ISRM 1985) using the value of normalized punching resistance, each of them as:

$$R_C = K\cdot I_{S(50)} \qquad R_T = I_{S(50)}/0{,}8$$

where K (multiplication coefficient) = 14 (Palmström 1995).

To proceed with the particle-size analysis, the mortars were first disaggregated with the use of a mortar and pestle, dried at 105 ± 5 ° C, weighed to measure the dry mass (m_{dM}), and then attached with acid solution (HNO_3, 13% vol.) for a period of immersion of 48 hours, so as to eliminate the carbonate binder matrix of the mortar. The samples were then filtered with Whatmann 41 paper, washed in distilled water, placed in an oven at 105 ± 5 ° C to determine the dry mass of the residual aggregate (m_{dR}) and, indirectly, the bulk mass of the binder (as: $m_{dB} = m_{dM}-m_{dR}$). Then, the particle-size distribution was performed using sieves series UNI 2131, with mesh opening of 4000, 2000, 500, 250, 125, 63 μm with sifter Giuliani IG3.

3. Results and discussion

3.1 Mineralogical and petrographic characteristics

Based on the observation macroscopic, the binder matrix of samples shows a colour from greyish to whitish (on fresh cut). The surfaces exposed directly to the weathering, due to the alteration (decarbonation, sulfation) show different colour, from ochre to grey more intense. In the zones of building exposed to the north, where not arrive the sun radiation, biological patinas are present, with a variable colour as function of species present (e.g., molds, mosses, lichens). In all mortar there are often lime lumps with different dimensions (from <1 to 7 mm), in some cases with radial fissuring or fractured.

The mineralogical and petrographic characteristics of the mortars (aggregate composition, binder reactivity with aggregate, aggregate/binder ratio) were defined by microscopic analysis in thin section, reported in Table 1.

The binder matrix is mainly constituted by microcrystalline calcite (Fig. 4), in which it is observed the presence of microporosity finely distributed in the paste.

In the aggregate of mortars different natural and artificial materials as natural gravel, sands or crushed were employed: volcanic rocks (and subordinately marble), crystal-clasts, cocciopesto fragments resulting from the grinding of various ceramic materials (bricks, tiles, pottery). These latter were used mainly in the wall and floor conglomerates.

In Table 2, irrespective of the composition, circularity data of aggregate are reported, determined with image analysis on thin section photographs by software ImageJ1.47v. Substantial differences in the circularity between the various types of mortar were not detected. It must be stressed that the data refer mainly to the aggregate component with size statistically <8 mm. They are therefore not counted coarse fragments, frequently found in the vault concretes (frequent size range: 30-150 mm, e.g. *caementia*) and cocciopesto conglomerates of walls and floors (frequent size range: 10-30 mm). Counting this part coarse aggregate (impossible due to the size limitation of the samples) in the latter surely the circularity value would considerably lower.

The volcanic aggregate is made from two kind of rocks: leucitic basalt and leucitites, belonging to the alkaline rocks of ultrapotassic serie (HKS) from the Roman Magmatic Province (Morbidelli 2003; Peccerillo 2005).

The first is represented mainly by two kind of scoria clasts (Fig. 4) with different colour: grey-black and grey-red. It has normally sub-spherical shape with porous and glassy appearance. Both types of leucitic basaltic aggregate are present in all mortar samples with high amounts (>65%; Tab. 1) with respect to total aggregate. It shows great similarity with the volcanic scoria outcropping around the Hadrian's Villa.

The texture of leucitic basalt is afiric. The paragenesis consists of clinopyroxene (Fig. 4), leucite, hornblende, opaque minerals (i.e. Ti-magnetite, magnetite), ± plagioclase. Rare biotite and olivine, often altered in iddingsite, are present. Having a glassy matrix, show edge of pozzolanic reaction with the binder (Fig. 4).

The leucitite agregate (Fig. 4) has a lower presence in the mortars with respect to leucitic basaltic scoria. It represents < 8% of total aggregate (Tab. 1). It has a greyish colour with shape normally subspherical (Tab. 2), show a low porosity and is frequently altered. The paragenesis is composed mainly by leucite, clinopyroxenes and opaque minerals, while the feldspars are rare or absent.

The crystal-clasts present in the aggregate of mortars consist essentially of hornblende, clinopyroxene, rare biotite.

The *cocciopesto* aggregate (Fig. 4; Tabs. 1, 2) has variable size of fragments with angular shape. It has a variable colour from yellow-ochre to pink-orange to rust-red, due to different compositions and fire conditions. As consequent, these ceramic products show variable physical characteristics (porosity, mechanical strenght; Columbu et al. 2015). Cocciopesto aggregate shows typical edge reaction with binder (Fig. 4). Observing the matrix, crystals of quartz and plagioclase are present immersed into the matrix. Rare leucitic basaltic fragments (< 5% on the total) and Fe-oxides (*e.g.* hematite) are present.

The mortar samples show the occasionally presence (in low amount) of white marble aggregate, normally with sharp edges. This aggregate is present mainly in the finishing plasters and, subordinately, in the bedding mortars of *cubilia*, brick walls and vault concretes.

In some samples, local pyroclastic rocks (belonging to Hadrian's Villa area) were used as coarse aggregate (4-10 mm) or *caementia* in the concretes (with frequently size: 5-20 cm). This rock is characterized by a glassy groundmass, lithic-clasts of varying particle-size with composition from leucitic-basaltic to leucititic, xenoliths (Fig. 4). Occasionally show typical alterations in zeolites and clay minerals (Peccerillo 2005). The accessory phases are iron and titanium oxides. Due to volcanic glass, these materials were used probably also as pozzolanic aggregate. In the aggregate of mortars it has been frequently detected the presence of the same crystal-clasts observed in the same pyroclastic rock (*i.e.*, green hornblende, clinopyroxene, biotite) as well as the leucitic basalt and leucitites.

3.2 Binder / aggregate ratio

According to Columbu et al. (2015) the ratio of binder and aggregate was initially calculated through image analysis on the six faces of the cube specimens. In Table 3 (first three columns) are reported the values.

The results show that this ratio varies depending on the specific function of the mortar in the spa. The average values for mortar group are higher in conglomerates in earthenware wall (*trullisatio*) (0.70; Tab. 3), and the brick mortars (0.68). The mortars and concretes of cubilia earthenware floor (*rudus*) have values of 0.62 ratio 0.59, respectively. Concretes of vaults show a lower average (0.54).

However, this ratio also varies within the individual samples of populations, thus showing a clear uniform due in the preparation of mortars.

For comparison, the mixing ratio between binder and aggregate has also been obtained through image analysis of photographs taken under a microscope (Tab. 3; Fig. 5). The values are always higher than those obtained by image analysis of cubic specimens (Tab. 3), due to different volumes of samples analysed in two cases.

In both cases, the values are higher than the values indicated by *Vitruvio* (Pollione 15 BC). According to his recommendations, the aggregate percentage in a mortar is a function mainly of particle-size distribution and the thickness of the mortar-cast. So, thickness of 1-2 cm provides an aggregate percentage of 65-70 vol.%, while thickness >2 cm provides an aggregate percentage of 70-80 vol.% (Cagnana 2000).

Based on the results obtained with both methods, the percentage of aggregate more similar to the recommendations of *Vitruvio* is the one obtained by image analysis on cubic specimens, but this is not perfectly correct because it does not detect the presence of aggregate with very small size (< 100 μm) undetectable by the image analysis.

Further values were calculated using weight ratio data (Tab. 4) after binder dissolution of the mortars made for determinate the particle size of aggregate, where is counted all aggregate fraction, also those less than 100 μm diameter. Data, as volume % of aggregate (Tab. 4) is very close to those recommended by Vitruvius (Tab. 5). This is mainly due to the different volumes of the samples (Tab. 6) with which the data were determined in three different ways, as shown in Fig. 5.

3.3 Composition of binder

The diffraction (XRPD) and thermo-gravimetric (TG/DSC) analysis on the fractions enriched in binder have provided information on the materials used and the secondary phases, allowing us to define the composition and hydraulic degree of the mortars.

Selected samples were analysed by X-ray Powder diffraction and patterns are shown in Fig. 7. In all samples the main Bragg reflections match with the database values for calcite ($CaCO_3$) phase. For ADTH 12C sample in addition, peaks (at 20.50, 21.63, and 23.29 2θ degrees) due to tridymite, peaks (at 21.96 and 28.42 2θ degrees) due to cristobalite and peaks due to quartz were also observed. Tridymite and cristobalite phases were not observed in the XRDP of the other samples. In these samples leucite ($KAlSi_2O_6$), muscovite ($KAl_2Si_3AlO_{10}(OH)_2$) phases were also observed. Others minor phases syngenite ($K_2Ca(SO_4)_2\cdot H_2O$) and quartz are also present. Quartz, leucite and mica (i.e., muscovite) belong to the phases of aggregate, from volcanic rocks (scoria and leucitite) and crystal-clasts.

In the XRDP patterns of ADTH 7 and ADTH 15 samples, peaks due to gypsum ($CaSO_4\cdot 2H_2O$) phase were present: in ADTH 7 sample peaks due to gypsum are very intense. Gypsum is due to sulfation processes, facilitated by the high open porosity calculated on the binder matrix.

Owing to the reactions between the binder and the pozzolan materials, between the hydraulic phases of new formation only small amount of an Ca/Al-silicate [i.e.: vuagnatite ($CaAlSiO_4(OH)$)] and ettringite ($(Ca_6Al_2(SO)_4(OH)_{12}\cdot 26H_2O$ have been identified by X-ray diffraction. The products of the pozzolanic reaction probably are present mainly as amorphous phases (gel-like C-S-A-H). Ettringite is formed as consequence of the chemical reaction between the sulphates and aluminates usually present in the hydration products of portland cement. Its formation depends on different factors: a) aluminates content), b) amount and origin of sulphates, c) quality of the mortar. Then, ettringite crystallisation involves a high increment of volume due to an expansive process with mortar disintegration (cracking and loss of mass).

The curves obtained with the TG/DSC simultaneous analysis (Figs. 8, 9) have typical trend of pozzolanic mortars (according to Branda et al., 2001). The curves show an initial loss of weight due to hygroscopic water below 120°C (Tab. 7). The observed gypsum phase in these XRDP patterns is in agreement with TGA result, where a net jump at 122 -150° C due to crystallized water loss of this phase is present in TGA curves of this samples. A following weight loss is present at temperatures between 480-500°C, probably associated with the reaction between calcium silicates and carbonates which liberate carbon dioxide according to the following chemical reaction:

$CaCO_3 + XSiO_2 \Rightarrow CaXSiO_3 + CO_2$ (where X = K, Al, F)

The loss in weight more extensive is recorded on the decomposition curve at temperatures between 550-600° and 800-830°C and is linked to the decarbonation reaction of Ca-carbonate ($CaCO_3 \Rightarrow CaO + CO_2$). From the curves it is observed that not all the samples have similar extension of the weight loss, showing a discrete compositional heterogeneity. The losses in weight percentages relative to the elimination of H_2O and CO_2 compounds (evaporation and decarbonation) are useful to trace pozzolanic activity of the sample analyzed.

The endothermic peaks (Fig. 9) of calorimetric curves (DSC) coincide to temperatures at which losses in weight in the TG curves are observed. Although the general meaning of different trends in thermic curves has not yet been clarified exhaustively, the losses in weight from low temperatures (~400°C) are due to reactions between calcium carbonate and silicates with formation of calcium silicates and production of CO2.

In DSC curves it is noteworthy that in the samples containing gypsum (wall-coatings mortars ADTH7, ADTH52; floor cocciopesto conglomerates ADTH15, plaster ADTH18 and ADTH58) it's observed an endothermic sharp peak due to dehydration of gypsum.

In some sample, in the range 480-500 °C it's observed a broad endothermic peak (evident in ADTH28 sample) due to the reaction between calcite and silicate to form Ca-silicate with develops carbon dioxide. This reaction may be also due to the presence of newly cement mortar residues of the restoration interventions in the last decades.

Finally, at higher temperatures (>600°C) in all the samples, the DSC curves have showed an increasing upward behaviour due to the incipient endothermic decomposition of calcite.

According to temperature ranges with characteristic losses in weight identified by Bakolas et al. (1995, 1998) and Moropoulou et al. (2000), in Fig. 10 have been reported CO_2 versus CO_2/H_2O ratio, where CO_2 is weight loss between

600÷800°C and H_2O is weight loss of bond water in the range of 200÷600°C (Tab. 8). Samples with the greater hydraulic degree are the mortars of marble flooring (CO_2 = 9.79%), followed by the vault concretes (CO_2 = 11.25%), *arriccio* plasters (CO_2 = 11, 65%), brick bedding mortars (CO_2 = 12.34%), and the coating bedding mortars (CO_2 = 12.74%). The lime-lumps being mainly compounds of Ca-idroxide/carbonate, have much higher values. The diagram shows an exponential correlation of data (R^2 = 0.95; Fig. 10).

3.4 Particle size analysis of aggregate

The cumulative distribution curves, obtained by sieving of the aggregate fraction (Tab. 9), demonstrate similar characteristics according to each mortar group (Figs. 11a, b, c, d, e, f, g, h, i). These curves shows how the aggregates used in the packaging of mortars derive in most cases from very fine gravel aggregate (also call granule) (Wentworth 1922), where the histograms of hold masses record the highest percentages at about 4000 and 2000 μm grain size sieves (Columbu et al. 2015). In other cases, where the frequency histogram recorded the highest held percentages on 2000 and 1000 μm these aggregates are defined as very coarse sand (Wentworth 1922). The morphology of the cumulative curves and the analysis of determinants diameters D_{10} and D_{60}, where possible, shows, in most of mortar groups a not uniform particle size and, in 2 cases, varied particle size (Figs. 11a, b, c, d, e, f, g, h). The non-uniform particle sizes are identified in bedding mortars of masonry elements such as bricks and *cubilia* (Figs. 11 a, b) where the ADTH4 and ADTH 42 samples deviate from the trend of other distribution curves. In these samples, the histograms indicate a modal class of 1000 and 2000 μm. The wall coating and floor coating mortars (Figs. 11a, b, c, d) show uniform grain sizes with similar cumulative curves with the exception of ADTH 28 and ADTH 37 samples that deviate slightly from the trend of the other group of samples. In these samples, the histograms indicate a modal class of 2000 and 1000 μm. Floors conglomerates (Fig. 11e) show a fairly similar morphology of the distribution curve as the plaster (Figs. 11h) However, for both groups the absence of determinant diameter D_{60} does not allow the classification according to the uniformity of particle's aggregate. The walls conglomerates are characterized by cumulative curves that showing a non-uniform particle sizes for the sample ADTH 18 and varied particles size for sample the ADTH26 (Figs. 11f). In vault concretes there is a great similarity of the cumulative curves that appear superimposed (Figs. 11g). The histograms of ADTH 12 and ADTH 50 samples presents a modal class of 2000 and 1000 μm, and cumulative curves presents a varied grain size for ADTH 50 sample. The sample ADTH 53 instead presents the classic characteristic particle size of most of the mortars with modal class to 4000, 2000 μm and not uniform grain size.

3.5 Physical-mechanical properties of mortars

3.5.1 Porosity, density and water absorption

Following physical and mechanical properties of bulk mortar samples (according to Columbu et al. 2015) were reported in Tab. 10: solid, real and bulk density**,** open and closed porosity to helium and water**,** weight imbibition coefficient**,** saturation index, punching strength index. Physical properties of binder and aggregates were reported on Table 11.

The physical properties show value dispersion, due to the different binder / aggregate mixture and relation between the size of aggregate and dimensions of bulk mortar specimens.

The porosity and bulk density, normally well correlated are good parameters to recognize the degree of compactness of a mortar, and also a good lay on the site. He open porosity varies from 34.14% to 51.19%, bulk density from 1.21 to 1.57 g/cm^3. In the diagram of Fig. 12a is possible to observe the different physical behaviour of the main mortar groups analysing the correlation coefficient (R^2).

The vault concretes, that not including the coarse aggregate (>15 mm, e.g., *Caementia*), bedding mortars of marble coatings, and bedding mortar of *cubilia* and bricks show coefficients medium-high (0.99, 0.81, 0.56, respectively), while the *cocciopesto* conglomerates show a lower value (0.31) due to the presence of the sample ADTH 58 with anomalous porosity.

Great variability of He open porosity and bulk density in the mortars is affected by also the binder and aggregate (Fig. 12a; Tab. 11), which show a large variability of these properties, ranging from 15.8 to 51.1% and from 0.38 to 1.61 g/cm^3 in the binder, from 13.7 to 48.0% and from 1.4 to 2.2 g/cm^3 in the aggregate.

Considering the mean values (Tabs. 10, 11), the less porous samples belong to the plaster (38.14%) and cocciopesto conglomerates (42.12 and 42.99%), which have low average values than other mortars (45-48%). These differences are evidently due to the different degree of compaction executed by the Romans (usually through the maces) in relation to mortar function in the building, as shown by the porosity data of binders, closely correlated with those of the porosity of the bulk mortar samples. Moreover, the presence of *cocciopesto* improves the hydraulic characteristics of the binder making it less porous.

Inside the group, the conglomerates of floor and wall show different value of these two parameters: 1.50 ± 0.07 g/cm^3 and 1.34 ± 0.13, respectively. Then, the first have a greater homogeneity also with respect to other mortars, resulting from a good homogeneity of the binders, with values of 0.77 ± 0.17 and 1.46 ± 0.48 and 0.64 ± 0.04 g/cm^3, respectively. Considered the structural function of the floor conglomerates. The binder homogeneity of floor conglomerates is probably due to a greater compaction (considered the structural function) and a use of *cocciopesto* aggregate with higher quality, characterized from lower porosity and greater bulk density.

However, the binders of mortars have a high variability of real density (Figs. 12b; Tab. 11) mainly influenced by the closed porosity and less by the solid density. In fact, it is conceivable that this latter remains unchanged (about 2.80 g/cm^3) in the samples analysed.

Contrary, the vault concretes and the bedding coating mortar show, for two different reasons, high porosity values. In the first case, since the thickness of the casting, it is due to a lower compaction or high amount of mixing water in the production of mortar. In the second case is due to the technical need to soft lay of the paving marble slabs.

In regard to the characteristics of water absorption, the imbibition coefficients (CI_W), closely related to weight He open porosity, highlight greater incidence of binder porosity (with coefficient correlation R^2 = 0.75, Fig. 13b; Tab. 11) with respect to the bulk mortar porosity (R^2 = 0.71, Fig. 13a; Tab. 10), including also the porosity created by aggregate immersed into the binder matrix. This is highlighted also by high imbibition coefficient of the ADTH 26 and 52 samples, which show great porosity (50% and 48%, respectively).

Saturation index (SI) of all mortar samples is always under the line of 100% (Fig. 14), forming a circumscribed sample population. Observing binder data, it's note the higher variability of saturation index with some samples near or over the line of 100%. This indirectly indicates: i) the presence of hygroscopic minerals (phyllosilicate, etc.) as evidenced by XRD analysis on enriched binder samples, ii) high heterogeneity of binder matrix, due to complexity geometry of porous network.

The volcanic aggregates (leucitic basalt and leucitites) show a saturation index close to 100% while the *cocciopesto* aggregates and *lateritious* fragments (bricks, tiles and crushed pottery) show lower average values of saturation index (Fig. 14; Tab. 11), probably due to a lower radius of porous (or greater tortuosity) with respect to the binder matrix and the bulk mortar samples.

For to understand better the physical-hydraulic behaviour of bulk mortars, in the Fig. 15 were reported the water absorption kinetic (Tab. 12).

3.5.2 Strength index and hydraulic degree of mortars

The physical mechanical characteristics (Tab. 13) of mortars and aggregate are shown in the Fig. 16a, where reported the punching strength index (Is_{50}) versus He open porosity, which show the well-known negative correlation.

The low punching index (with value <1 MPa) and the very low correlation (R^2= 0.20) with helium open porosity indicate that the resistance of mortars is affect by different factors: i) the porosity of bulk mortar sample; ii) small dimensions of the specimens respect to aggregate size; iii) characteristics of the binder (*i.e*., cohesion degree, porosity, etc.). However, it's possible made some evaluations. Except the plasters, the floor conglomerates and bedding mortars show the greater mechanical resistances (0.53 ± 0.26 and 0.49 ± 0.24 MPa, respectively; Tabs. 10, 13) with respect to other mortars (range 0.25-0.28), probably due to a presence of an aggregate with high quality, as evidenced by physical data of the *lateritious* samples from *Heliocaminus* Baths and "Grandi Terme" Baths (Columbu et al. 2015). The higher resistance of the plasters respect to other mortars can be explained with a lower helium open porosity (38.14 ± 2.13%; Tab. 10) and a higher bulk density (1.54 ± 0.01 g/cm^3), probably due to better mixing of binder-aggregate.

The diagram of Fig. 16b, where reported strength index versus CO_2/H_2O (which represent a good parameter inversely correlated with hydraulicity), highlight a negative correlation between the hydraulic degree of mortars and mechanical resistance, as evidenced by correlation coefficient (R^2 = 0.57; Fig 16c) in which were excluded the mortars with coarse aggregate.

Overall, the physical-mechanical tests show that the strength of mortars depends on: i) porosity of bulk mortar sample, represented by discontinuities between aggregate and binder, and porous binder matrix; ii) hydraulic degree of mortar; iii) sorting degree and particle size of the aggregate (see samples ADTH 4, 42, 54, from bedding mortars of brick and *cubilia*, characterised by higher sorting with modal class between 2000 and 1000 microns, than other mortars with modal class on class 4000 microns). Subordinately, the mechanical resistance depends on: i) size ratio of aggregate / specimen; ii) thickness of mortars, as evidenced by low values in the vault concretes and high strengths in the *arriccio* plasters.

4. Conclusions

The results highlight that the construction of the Heliocaminus baths respects the general architectural and structural issues of Roman period. This ancient building was constructed using mainly bricks and volcanic stones (i.e., *cubilia* for ashlars) outcropping within the area of Hadrian's Villa.

For aggregate of mortars were used volcanic rocks, cocciopesto and crystal-clasts. Volcanics consist mainly of red and black leucitic basaltic scoria and subordinately leucitites belonging to the alkaline rocks of ultrapotassic series of the Roman Magmatic Province, outcropping around the area of the Hadrian's Villa. Only basaltic scoria aggregate reacted with binder, while the leucitites did not show reactivity, because is not present glass in the matrix.

For conglomerates (*trullisatio* and *rudus*) and plasters (*arriccio*) was used also the *cocciopesto*, with medium-coarse particle-size (frequenty range: 6-30 mm), while in the floor marble-coating mortars was used a cocciopesto aggregate with smaller size (<8 mm). As evidenced by different physical properties, the cocciopesto show different quality, as function of kind and quality of ceramic material crushed (e.g., bricks, pottery, tiles). In any case, as shown by reactions borders with the binder, the *cocciopesto*, together the glassy volcanic scoria, gives good pozzolanic characteristics to the mortars.

The diffraction (XRPD) and thermal (TG/DSC) analysis on the fractions enriched in binder highlight that the binder consists mainly of calcite. Quartz, leucite and mica (i.e., muscovite), are all present as residual phases of aggregate. Owing to the pozzolanic reactions, the hydraulic phases of new formation have not been identified by X-ray diffraction, due to their small amount and, therefore, because probably are amorphous phases (gel-like C-S-A-H).

Gypsum and ettringite are sporadically present, indicating an advanced alteration degree. The first is due to sulfation processes, facilitated by the high open porosity calculated on the binder matrix. Ettringite is formed as consequence of the chemical reaction between the sulphates and aluminates present in the hydration products.

The use and mode of mixing of aggregate and binder in the production of mortar are made according to the Roman standard methods known at the time, with different mixtures in relation to the function in the masonry as well as suggested by *Vitruvio*.

Despite this, the physical-mechanical analysis show low values of punching strength index with respect to the standards of other Roman mortars. The low values depend mainly on high porosity of bulk mortar, due to a evident chemical-physical decay by: i) dissolution of the binder; ii) hydration / dehydration / crystallization of gypsum, ettringite, etc. that involves a high increment of volume with mortar disintegration (cracking and loss of mass). Except for the mortars of the cocciopesto-conglomerates, the low mechanical resistance can also be due to an occasional not perfect lay of mortars or completely mixing of aggregate with binder. Despite the low values, using CO_2/H_2O ratio data of TG/DSC analysis a good positive correlation (R^2 = 0.57) between hydraulic degree and mechanical strength was found, showing the important function of pozzolanic aggregate in the mortars.

The high variability of some physical properties (bulk density, porosity, particle size of aggregate), in some cases within groups of samples, together the short time of baths construction, show that the production and processing of the mortars were made quickly, probably also in discontinuous ways with changes of the workforce.

This latter lets to imagine that that there may have been many small construction phases. Then, considering that the complex represents an “experimental building”, with an attempt to test new solutions in re-invention of architectonic spaces, these several construction phases can would related to rethinking during the design and organization of various spaces or the functionality of the baths (*e.g.*, heating system, where the furnaces beneath the *sudatio* room have never been used for significant periods).

These construction evidences were highlighted by an accurate digital survey (Columbu et al. 2015) that supports the theory of a building of new conception, with advanced technical solutions, in some cases with poor results, with numerous changes in technical and building solutions.

Acknowledgements

Thank to Dr. Benedetta Adembri of the “Soprintendenza per i Beni Archeologici del Lazio” for the support and collaboration, Giorgio Verdiani, Dipartimento di Architettura of the Florence University (UNIFI), Italy, responsile of operative group of digital survey.

References

Adam JP (2006) L’arte di costruire presso i romani, materiali e tecniche vol 10. Longanesi

Adriano P, Santos Silva A, Veiga R, Mirão J, Candeias AE (2009) Microscopic characterization of old mortars from Santa Maria Church in Énvora. Material Characterization 60,7:610-620

Attanasio D, Bruno M, Prochaska W, Yavuz AB (2013) The Asiatic marbles of the Hadrian's Villa at Tivoli. Journal of Archaeological Science 40:4358-4368

Attanasio D, Mesolella G, Pensabene P, Platania R, Rocchi P (2009) EPR and petrographic provenance of the architectural white marbles of three buildings at Villa Adriana. In: Maniatis Y (Ed.), Asmosia VII. Proceeding 7th International Conference ASMOSIA, Thassos 2003, Bulletin de Correspondance Hellenique Sup., 51, Athens, pp. 57-369

Babini C, Fiori C (1996) Impiego delle analisi termiche nello studio delle malte, stucchi, intonaci e finiture murarie, Mosaico-analisi dei materiali e problematiche del restauro parte 2. CNR - Consiglio Nazionale Delle Ricerche, Ravenna

Bakolas A, Biscontin G, Moropoulou A, Zendri E (1998) Characterization of structural byzantine mortars by thermogravimetric analysis. Termochimica Acta volume 321 1,2:151-160

Bultrini G, Fragala I, Ingo GM, Lanza G (2006) Minero-petrographic, thermal and microchemical investigation of historical mortars used in Catania (Sicily) during the XVII century A.D. Applied Physics A 83,4:529-536

Cagnana A (2000) Archeologia dei materiali da costruzione. SAP Società Archeologica S.r.l., Mantova

Cicerchia P (1985) Sul carattere distributivo delle terme con Heliocaminus di Villa Adriana. Xenia 9:47-60

Columbu S, Antonelli F, Lezzerini M, Miriello D, Adembri B, Blanco A (2014a) Provenance of marbles used in the Heliocaminus Baths of Hadrian's Villa (Tivoli, Italy). Journal of Archaeological Science 49: 332-342

Columbu S, Gioncada A, Lezzerini M, Marchi M (2014b) Hydric dilatation of ignimbritic stones used in the church of Santa Maria di Otti (Oschiri, northern Sardinia, Italy). Ital. J. Geosci. 133: 149-160

Columbu S, Sitzia F, Verdiani G (2015) Contribution of petrophysical analysis and 3D digital survey in the archaeometric investigations of the Emperor Hadrian’s Baths (Tivoli, Italy). Rendiconti Lincei 26,4:455-474

Columbu S, Verdiani G (2011) From the small elements to the urban scale: An investigation where petrophysical study of materials and architectural shape analysis try to read a masterplan in the Hadrian’s Villa, Tivoli (Rome, Italy). In: Proceedings of 16th International Conference on Cultural Heritage and New Technologies (CHNT 2011) Wien. 14-16 november 2011, Urban Archaeology and Prospection, Museen der Stadt Wien – Stadtarchäologie. eBook Ed., vol. 1, part 3, pp. 273-293

Columbu S, Verdiani G (2014) Digital Survey and Material Analysis Strategies for Documenting, Monitoring and Study the Romanesque Churches in Sardinia, Italy, Lecture Notes in Computer Science, Springer 8740: 446-453

Crisci GM, De Francesco AM, Gagliardi F, Mercurio P, Gattuso C, Miriello D. (2002) L’analisi composizionale delle malte: Un valido mezzo per risalire alle fasi costruttive. Risultati preliminari. In Proceedings of II Congresso nazionale di archeometria, pp 485-494

Crisci GM, De Francesco AM, Gagliardi F, Mercurio P, Miriello D (2001) L’analisi composizionale delle malte: metodo di studio delle fasi costruttive in architettura. Arkos 4:34-41

De Luca R, Cau Ontiveros MA, Miriello D, Pecci A, Le Pera E, Bloise A, Crisci GM (2013) Archaeometric study of mortars and plasters from the Roman City of Pollentia (Mallorca-Balearic Islands). Per. Mineral. 82: 353-379

Drdácky M, Fratini F, Frankeová D, Slízˇková Z (2013) The Roman mortars used in the construction of the Ponte di Augusto (Narni, Italy) A comprehensive assessment. Construction and Building Materials 38:1117-1128

Giuliani Cairoli F (2006) L’edilizia nell’antichità. Carocci, Roma

ISRM International Society For Rock Mechanics (1972) Suggest method for determining the point load strength index. ISRM (Lisbon, Portugal). Committee on field tests. Document n.1, pp. 8-12

ISRM, International Society For Rock Mechanics (1985) Suggest method for determining the point load strength. ISRM commis- sion for testing methods, Working group on revision of the point load

Lapuente P, León P, Nogales T, Royo H, Preite-Martinez M, Blanc Ph (2012) White sculptural materials from Villa Adriana: study of provenance. In: Gutiérrez Garcia A, Lapuente P, Rodà I (Eds.), Interdisciplinary Studies on Ancient Stone. Proceedings of the IX ASMOSIA Conference, Tarragona, pp. 364-375

Lezzerini M, Antonelli F, Columbu S, Gadducci R, Marradi A, Miriello D, Parodi L, Secchiari L, Lazzeri A (2016) The Documentation and Conservation of the Cultural Heritage: 3D Laser Scanning and Gis Techniques for Thematic Mapping of the Stonework of the Façade of St. Nicholas Church (Pisa, Italy). International Journal of Architectural Heritage: Conservation, Analysis, and Restoration, 10,1:9-19.

Mac Donald WL, Pinto JA (2006) Villa Adriana: la costruzione e il mito da Adriano a Louis I. Kahn. Electa Architettura Paperback, Milano

Maravelaki-Kalaitzaki P, Bakolas A, Moropoulou A (2003) Physico-chemical study of Cretan ancient mortars. Cem. Concr. Res. 33:65-61

Miriello D, Antonelli F, Apollaro C, Bloise A, Bruno N, Catalano E, Columbu S, Crisci GM, De Luca R, Lezzerini M, Mancuso S, La Marca A (2015) New data about the ancient mortars from the archaeological site of Kyme (Turkey): compositional characterization. Per. Mineral. 84:497-517.

Miriello D, Barca D, Bloise A, Ciarallo A, Crisci GM, De Rose T, Gattuso C, Gazineo F, La Russa F (2010a) Characterisation of archaeological mortars from Pompeii (Campania, Italy) and identification of construction phases by compositional data analysis. Journal of Archaeological Science 37:2207-2223

Miriello D, Bloise A, Crisci GM, Apollaro C, La Marca A (2011) Characterization of archeological mortars and plasters from Kyme (turkey). Jurnal of archeological science 38:794-804

Miriello D, Bloise A, Crisci GM, Barrese E, Apollaro C (2010b) Effects of milling: A possible factor influencing the durability of historical mortars. Archaeometry 52,4:668–679

Morbidelli L (2003) In: Le rocce e i loro costituenti. Bardi Editore, Roma

Moropoulou A, Bakolas A, Aggelakopoulou E (2003a) Evaluation of pozzolanic activity of natural and artificial pozzolans by thermal analysis. Thermochimica Acta 420:135-140

Moropoulou A, Bakolas A, Bisbikou K (1995) Characterization of ancient, byzantine and later historic mortars by thermal and X-ray diffraction techniques. Termochimica Acta 269-270:779-795

Moropoulou A, Bakolas A, Bisbikou K (1999) Investigation of the tecnology of hystoric mortars, Journal of cultural heritage 1:45-58

Moropoulou A, Polikreti K, Bakolas A, Michailidis P (2003b) Correlation of physicochemical and mechanical properties oh historical mortars and classification by multivariate statistics. Cement and concrete research 33:891-898

Moropoulou, A., Bakolas, A., Aggelakopoulou, E. (2004). Evaluation of pozzolanic activity of natural and artificial pozzolans by thermal analysis. Thermochimica Acta, 420:135-140.

Moropoulou, A., Bakolas, A., Anagnostopoulou, S. (2005). “Composite materials in ancient structures”, Cement and Concrete Composites, 27:295–300.

Moropoulou, A., Bakolas, A., Bisbikou, K. (2000). Investigation of the technology of historic mortars. Journal of Cultural Heritage, 1:45–58.

Moropoulou, A., Bakolas, A., Moundoulas, P., Aggelakopoulou E., Anagnostopoulou, S. (2013). Optimization of compatible restoration mortars for the earthquake protection of Hagia Sophia. Journal of Cultural Heritage, 14S:147-152.

Moropoulou, A., Cakmak, A.S., Biscontin, G., Bakolas, A., Zendri, E. (2002). Advanced Byzantine cement based composites resisting earthquake stresses: the crushed brick/lime mortars of Justinian's Hagia Sophia. Construction and building materials, 16, 543–552.

Ortega LA, Zuluaga MC, Olazabal A (2008) Geochemical characterization of archaeological lime mortars: Provenance inputs. Archaeometry 50,3:387-408

Palmstrom A (1995) RMi-a rock mass characterization system for rock engineering purposes. Ph D. thesis. University of Oslo, Norway

Palomo A, Blanco-Varela MT, Martinez-Ramirez S, Puertas F, Fortes C (2011) Historic mortars: Characterization and durability. New tendencies for research. Eduardo Torroja Institute, Madrid

Papayianni I, Pachta V, Stefanidou M (2013) Analysis of ancient mortars and design of compatible repair mortars: The case study of Odeion of the archaeological site of Dion. Construction and Building Materials, 40:84-92

Peccerillo A (2005) Plio-Quaternary volcanism in Italy. Petrology, Geochemistry, Geodynamics. Springer, Heidelberg

Pensabene P, Antonelli F, Lazzarini L, Cancelliere S (2012) Provenance of marble sculptures and artifacts from the so-called Canopus and other buildings of “Villa Adriana” (Hadrian’s Villa, Tivoli, Italy). Journal of Archaeological Sciences 39: 1331-1337

Pollione MV (15 BC) De Architecture. Vol. II. In: Cesariano C, De Architectura Libri Dece, 1521, Como

Riccardi MP, Duminuco P, Tomasi C, Ferloni P (1998) Thermal, microscopic and X-ray diffraction studies on some ancient mortars. Thermochimica Acta 321:207-214

Salza Prina Ricotti M (2000) Villa Adriana il sogno di un imperatore: Architettura, arte e giardini. L’Erma di Bretschneider, Roma

Smith P, Smith RM (2009) Bricks and Mortar: A Method for Identifying Construction Phases in Multistage Structures. Historical Archaeology 43:40-60

Stanislao C. Rispoli C. Vola G. Cappelletti P. Morra V. De Gennaro M (2011) Contribution to the knowledge of ancient Roman seawater concretes: Phlegrean pozzolan adopted in the construction of the harbour at Soli-Pompeiopolis (Mersin, Turkey). Periodico di Mineralogia 80,3:471-488

Topçu IB, Isıkdag B (2013) The effect of ground granulated blast-furnace slag on properties of Horasan mortar Burak Ißsıkdag. Construction and Building Materials 40:448-454

Verdiani G, Columbu S, (2010) E. Stone, an archive for the Sardinia monumental witnesses. Third International Conference, EuroMed 2010, Lemessos, Cyprus, November 8-13, 2010. Book Chapter. 'Lecture Notes in Computer Science' (LNCS), Springer. Berlin-Heidelberg Vol. 6436:356-372

Verduchi P (1975) Le Terme con cosiddetto Heliocaminus a Villa Adriana. Quaderni dell’Istituto di Topografia Antica 8:55-95

Vola G, Gotti E, Brandon C,Oleson JP, Hohlfelder RL (2011) Chemical, mineralogical and petrographic characterization of roman ancient hydraulic concretes cores from Santa Liberata, Italy, and Caesarea Palestinae, Israel, Periodico di mineralogia 80,2:317-338

Wentworth CK (1922) A scale of grade and class terms for clastic sediments. J. Geology 30:377-392

Captions of Figures

Fig. 1 (a) Photo-overwiew of 3D model of Hadrian's Villa (made by Italo Gismondi, 1956), where highlights the *Heliocaminus* bath (on the central-left); (b) View of *Heliocaminus* room; (c, d) Natatio room.

Fig. 2 *Heliocaminus* Baths: (a) mortar of brick wall; (b) wall of Natatio masonry room with *cubilia* bedding mortar; (c) internal view with mortars of floor (down) and wall (in front) coating for slab marble; (d) detail of sample ADTH 7 od wall coating mortar; (e) floor conglomerates with cocciopesto (suspensura); (f) wall coating and conglomerates with cociopesto of *Frigidarium* room; (g) vault concretes of collapsed vault; (h) wall with plaster (sample ADTH 14).

Fig. 3 Map of *Heliocaminus* Baths with sampling points of mortars.

Fig. 4 Micro-photographs on thin section of mortars and aggregates: (a) cross Nicol: phenocrysts immersed in microcrystalline ground mass in the leucitic basalt; (b) plain polars: leucite crystals in the leucitites; (c, d) plain polars: vesicular black and red scoria with binder reaction border; (e, f) plain polars: vesicular black scoria and cocciopesto fragments with reaction border with binder; (g, h) vesicular black scoria with obvious reaction border with binder (inside scoria fragment there are two leucite crystals).

Fig. 5 Microphotographs on mortar thin section realised with binarization and filling holes options by image analysis with software ImageJ 1.47v. (a) brick mortar; (b) cubilia mortar; (c) floor coating mortars; (d) wall coating mortar; (e) floor conglomerate; (f) wall conglomerate; (g) vault concrete; (h) plaster.

Fig. 6 Comparison of three different methods (by image analysis on thin section and on cubic bulk mortar specimens, and using weight data from acid dissolution of binder mortar for determinate the particle size analysis) to calculate the binder / aggregate ratio as vol% using different sample volume.

Fig. 7 Qualitative mineralogical analysis of binder (XRPD): diffractograms of aerial and hydraulic mortars.
XRDP pattern for selected samples. The dotteds curves are the experimental data. The lower vertical bars represent reflection positions of major and common components: calcite (PDF card 5-586), gypsum (PDF card 21-816), leucite (PDF card 71-1147), muscovite (PDF card 7-25) and ettringite (PDF card 41-1451) phases.
Abbreviations: Cc = calcite; Qz = quartz; Crd = cristobalite; Trd = tridymite.

Fig. 8a Thermo-gravimetric analysis on the enriched binder fraction of mortars. TG curves: mass loss (%) versus temperature in celsius degrees. (a) brick mortar; (b) cubilia mortar; (c) floor coating mortars; (d) wall coating mortar.

Fig. 8b Thermo-gravimetric analysis on the enriched binder fraction of mortars. TG curves: mass loss (%) versus temperature in celsius degrees. (e) floor conglomerate; (f) wall conglomerate; (g) vault concrete; (h) plaster; (i) lump.

Fig. 9 Differential scanning calorimetric (DSC) curves related to the enriched binder fraction of mortars. Heat flow *versus* temperature.

Fig. 10 Diagram CO_2 *versus* CO_2/H_2O ratio for mortars of Heliocaminus Baths, where CO_2 is weight loss (%) between the temperature range of 600÷800°C and H_2O is weight loss of bond water in the range of 200÷600°C (from Moropoulou *et al*. 2000, modified).

Fig. 11 Particle-size distribution (Log grain diameter *versus* cumulative passing %) of each mortar group with different function in the *Heliocaminus* Baths.

Fig. 12 Physical properties of mortars, binders and aggregates: (a) helium open porosity (Φ_OHe) *versus* bulk density (ρ_B); (b) real density (ρ_R) *versus* helium closed porosity (Φ_OHe).

Fig. 13 Physical properties of mortars, binders and aggregates: (a) helium open porosity (Φ_OHe) *versus* imbibition coefficient (CI_W) of mortars; (b) helium open porosity (Φ_OHe) *versus* imbibition coefficient (CI_W) of binders and aggregates.

Fig. 14 Physical properties of mortars, binders and aggregates: helium open porosity (Φ_OHe) *versus* water open porosity ($\Phi_O H_2O$), reporting the line of saturation index at 100%.

Fig. 15 Physical properties of mortars: absorption kinetics for each mortar group, where reported Time (h) *versus* water absorption (progressive CI_W).

Fig. 16 Physical properties of mortars, binders and aggregates: (a) helium open porosity (Φ_OHe) *versus* Point Load Strength index (Is_{50}) of all mortars; (b) CO_2 / H_2O *versus* Point Load Strength index (Is_{50}) of all mortars and lumps; (c) CO_2 / H_2O *versus* Point Load Strength index (Is_{50}) of bedding mortars and lumps.

Captions of Tables

Table 1. Compositional characteristics by microscopic analysis of the mortars from the *Heliocaminus* Baths, where reported: localization, sampling height, % distribution of different aggregates.

Table 2. Circularity data of mortar aggregate of mortars determined by image analysis on thin section, where reported: circularity variation range, average, mean of average circularity data, standard deviations, variation coefficient.

Table 3. Comparison data of binder / aggregate ratio of all mortars determined on three different methods: by image analysis on thin section and on cubic bulk mortar specimens, and using weight data from acid dissolution of binder mortar for determinate the particle size analysis. Abbreviations: B = binder, A = aggregate.

Table 4. Data for calculate the aggregate ratio using the compositional distribution, determined by microscopic analysis, and weight data after dissolution of binder used for made the particle size analysis. Abbreviations: B = binder, A = aggregate.

Table 5. Comparison data of aggregate vol% of all mortars determined on three different methods with mortar thickness and values of B / A recommended by Vitruvio. Abbreviations: B = binder, A = aggregate.

Table 6 Data used for made the graphic of Fig. 6, where reported bunder / aggregate ratio (determine by vol.) and specimen volume (in cm^3).

Table 7 Thermo-gravimetric analysis: weight % difference data of enriched binder samples in the following temperature ranges: 25-120°C, 120-200°C, 200-400°C, 400-600°C, 600-850°C.

Table 8 Thermogravimetric analysis data of the mortars, where reported mass losses (%) for temperature ranges. The CO_2 (and H_2O) values were obtained using the TG curves, considering the temperature range in which the decarbonation reaction occurs.

Table 9 Particle size analysis of aggregate: data of cumulative passing % with cumulative passing masses (%) to following sieve series: 63, 125, 250, 500, 1000, 2000, 4000 μm.

Table 10 Physical properties of mortars (from Columbu et al. 2015, modified).
Abbreviations: S.D. = standard deviation; ρ_R = real density; ρ_B = bulk density; Φ_OHe = helium open porosity; $\Phi_O H_2O$ = water open porosity; CI_W = water imbibition coefficient; SI = water saturation index; Is_{50} = Point Load strength index.

Table 11 Physical properties of binders and aggregate (from Columbu et al. 2015, modified). The physical properties were determined indirectly using the physical properties of the mortars and composition percentages of aggregates determined by modal analysis (Table ESM2), according to the following general formula:

$X_n (B) = [X_n (M) - (X_{n (a)}•\%_{(a)}) - (X_{n (b)}•\%_{(b)}) - (X_{n (c)}•\%_{(c)}) - (X_{n (d)}•\%_{(d)}) - (X_{n (e)}•\%_{(e)}) - (X_{n (f)}•\%_{(f)})] / \% (A)$

Abbreviations: S.D. = standard deviation; X = physical properties; (M) = mortar; (B) = binder; (A) = aggregate; n = number from 1 to 6 of different physical properties. with X_1 = real density; X_2 = bulk density; X_3 = He open porosity; X_4 = H_2O open porosity; X_5 = He closed porosity; X_6 = imbibition coefficient; ρ_R = real density; ρ_B = bulk density; Φ_OHe = helium open porosity; Φ_CHe = helium closed porosity; Φ_T = total porosity; $\Phi_O H_2O$ = water open porosity; CI_W = water imbibition coefficient; SI = water saturation index; (a) = scoria; (b) = leucitite; (c) = *cocciopesto*; (d) = marble; (e) = clinopyroxene; (e) = green hornblende; (f) = biotite. The saturation index of binders is calculated as: SI = $(\Phi_O H_2O/\Phi_O He)$ •100. The solid density of binder is assumed to 2.80 g/cm^3 as average of literature data.

Table 12 Kinetic water-absorption curves determinate for total immersion on cubic bulk specimens with weight measurements of sample every 24 hours.

Table 13 Data of Point Load Test for determination of punching strenght index (Is_{50}) on cubic bulk specimens of mortars. Abbreviations: Distance between two punches (higher of specimen); W = specimen width; 2L = specimen length; P = ripture load; A = WD = section of rupture, of the specimen; De = equivalent diameter; $Is_{(50)}$ = PLT strength index; Rc = theoretical compression strength; Rt = theoretical tensile strength (according to ISRM, International Society For Rock Mechanics, 1985).

Figure 1

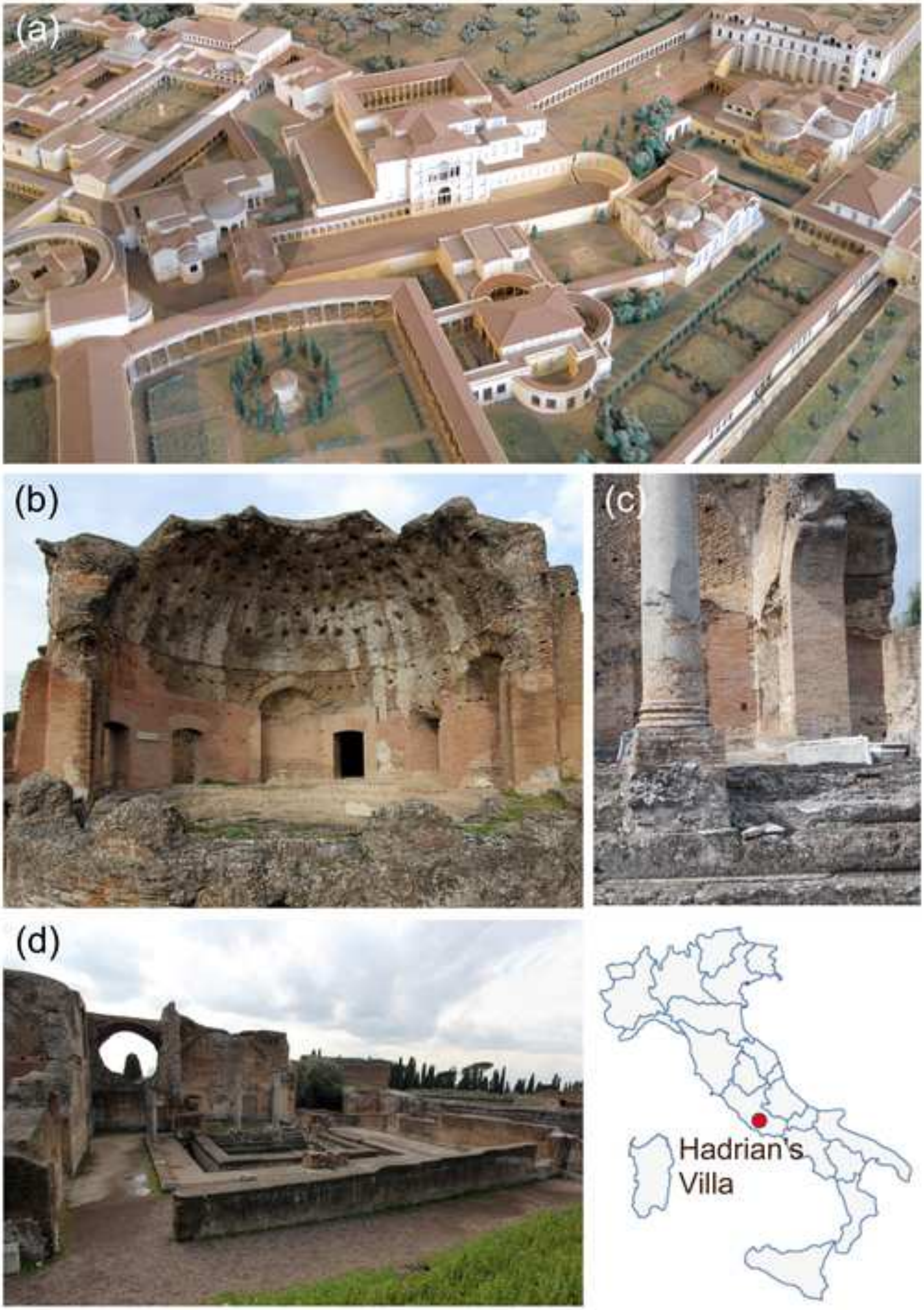

Figure 2

Figure 3

Click here to download Figure Figure 3.tif

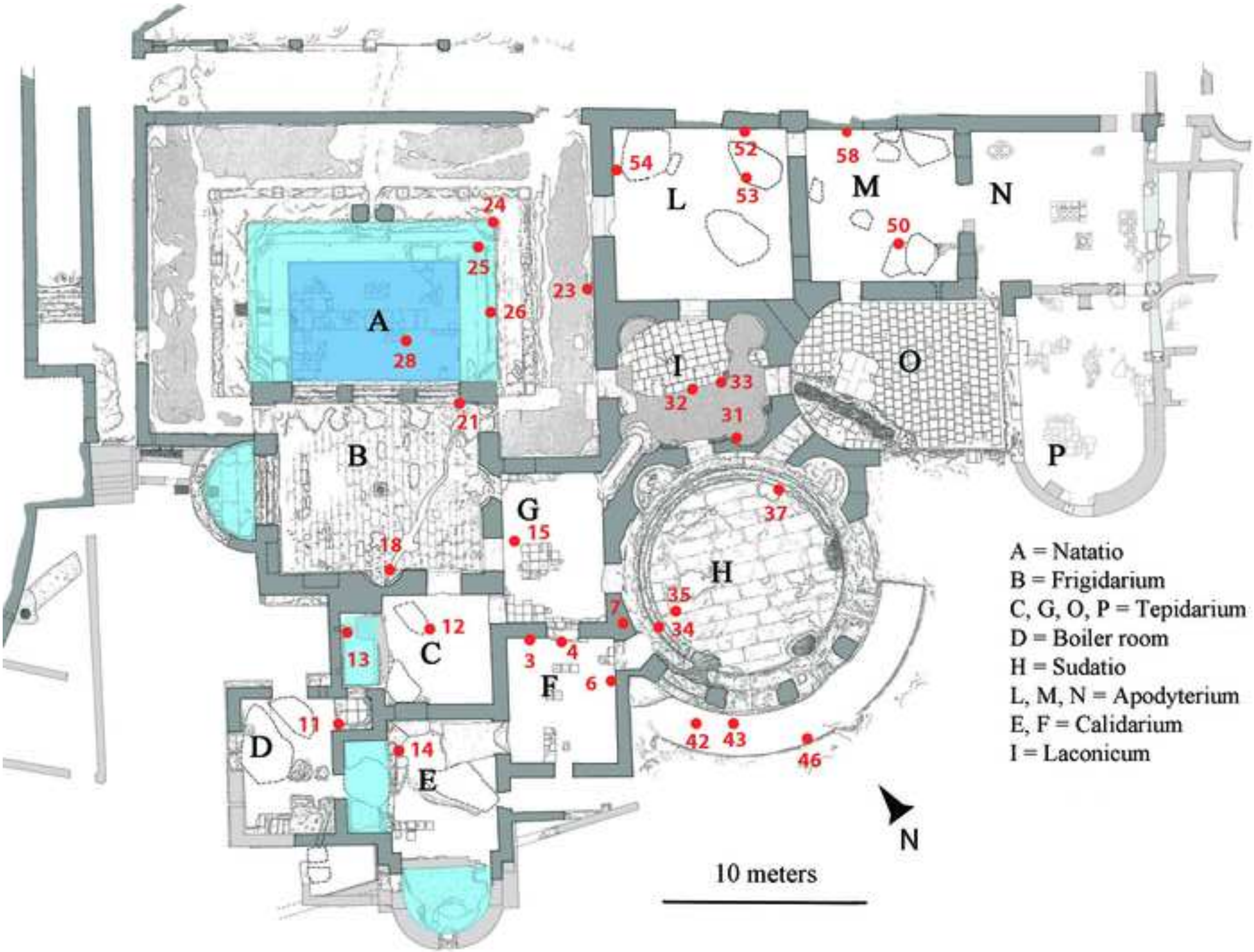

Figure 4

Click here to download Figure Figure 4.tif

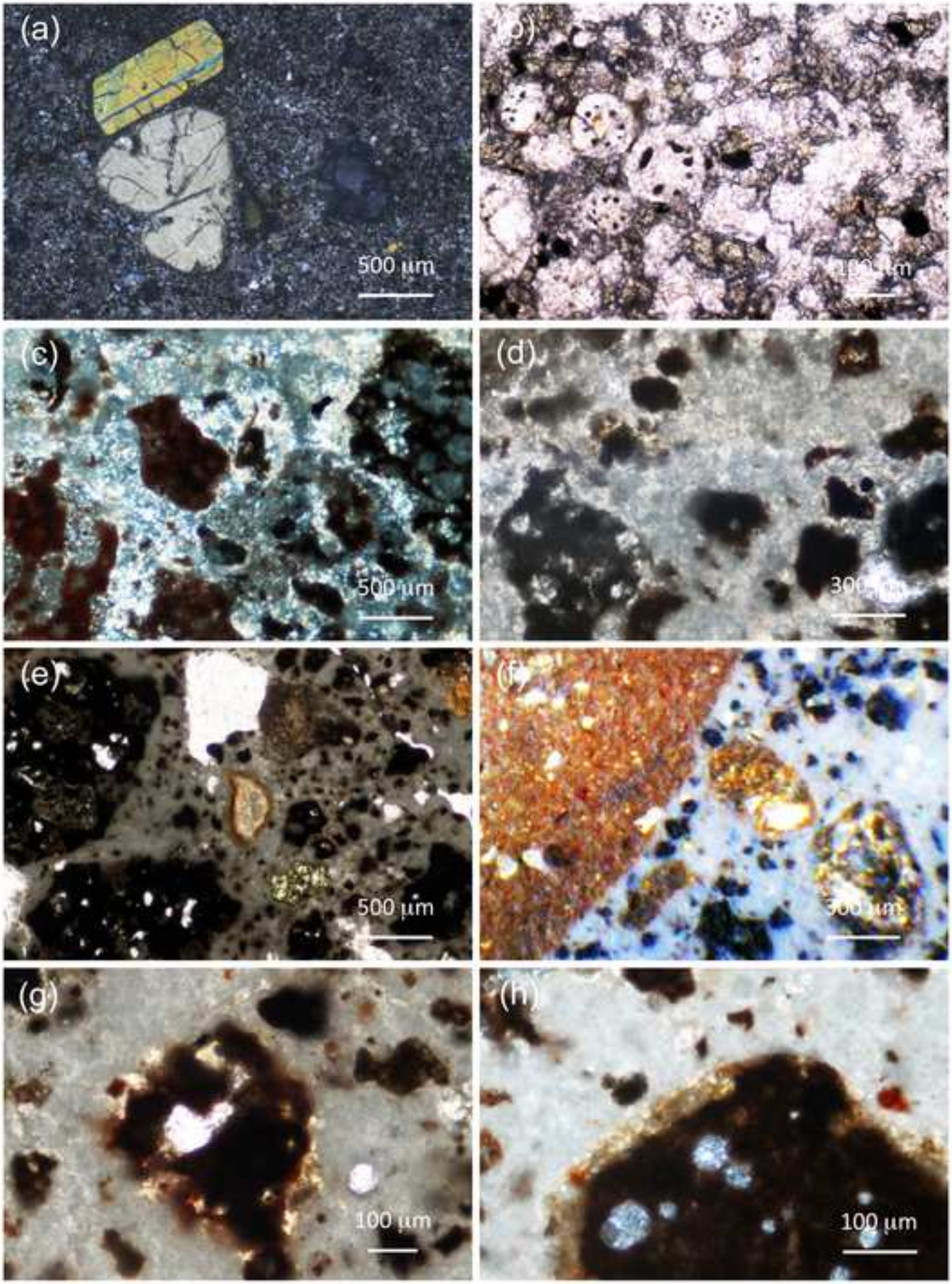

Figure 5

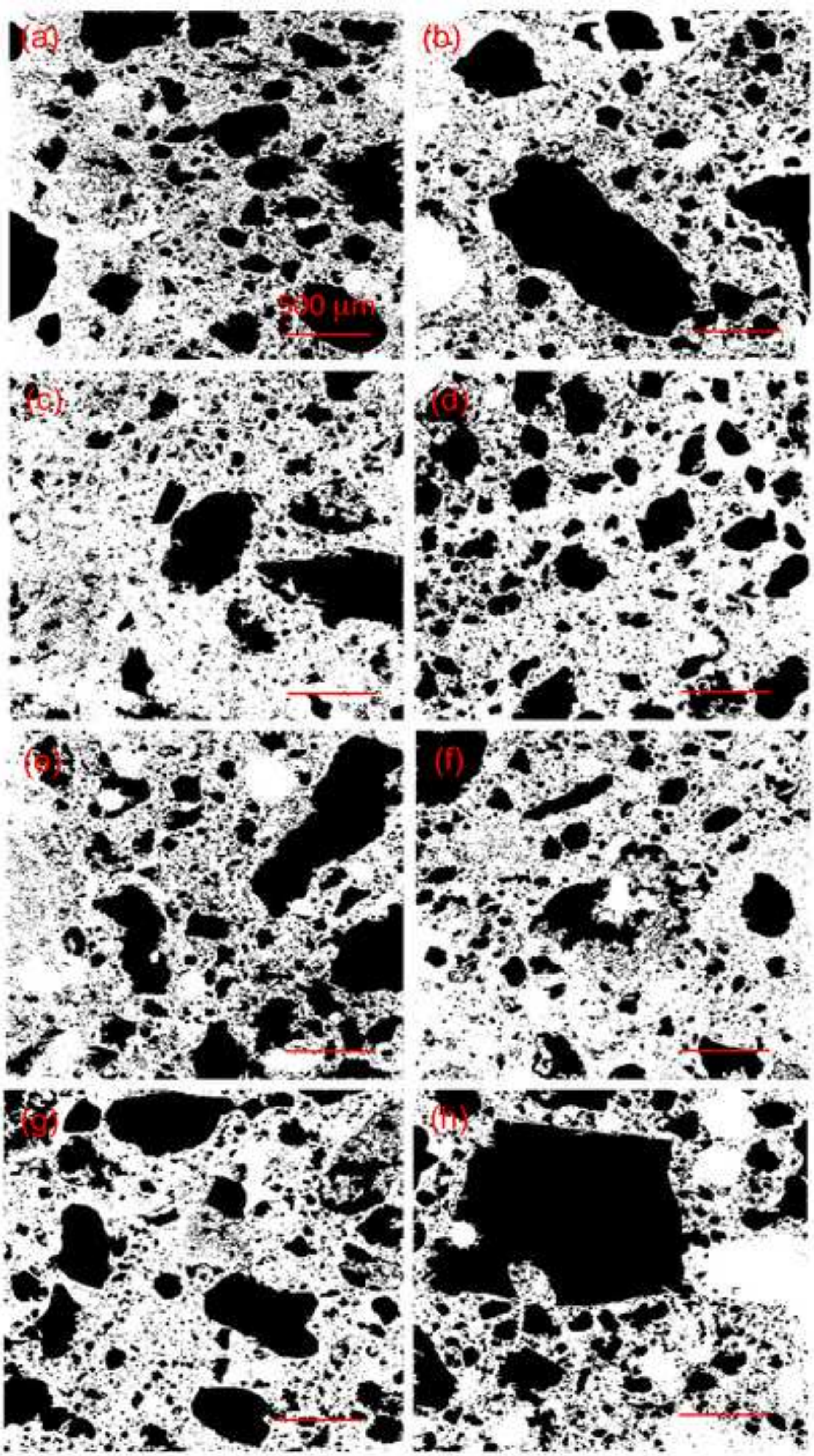

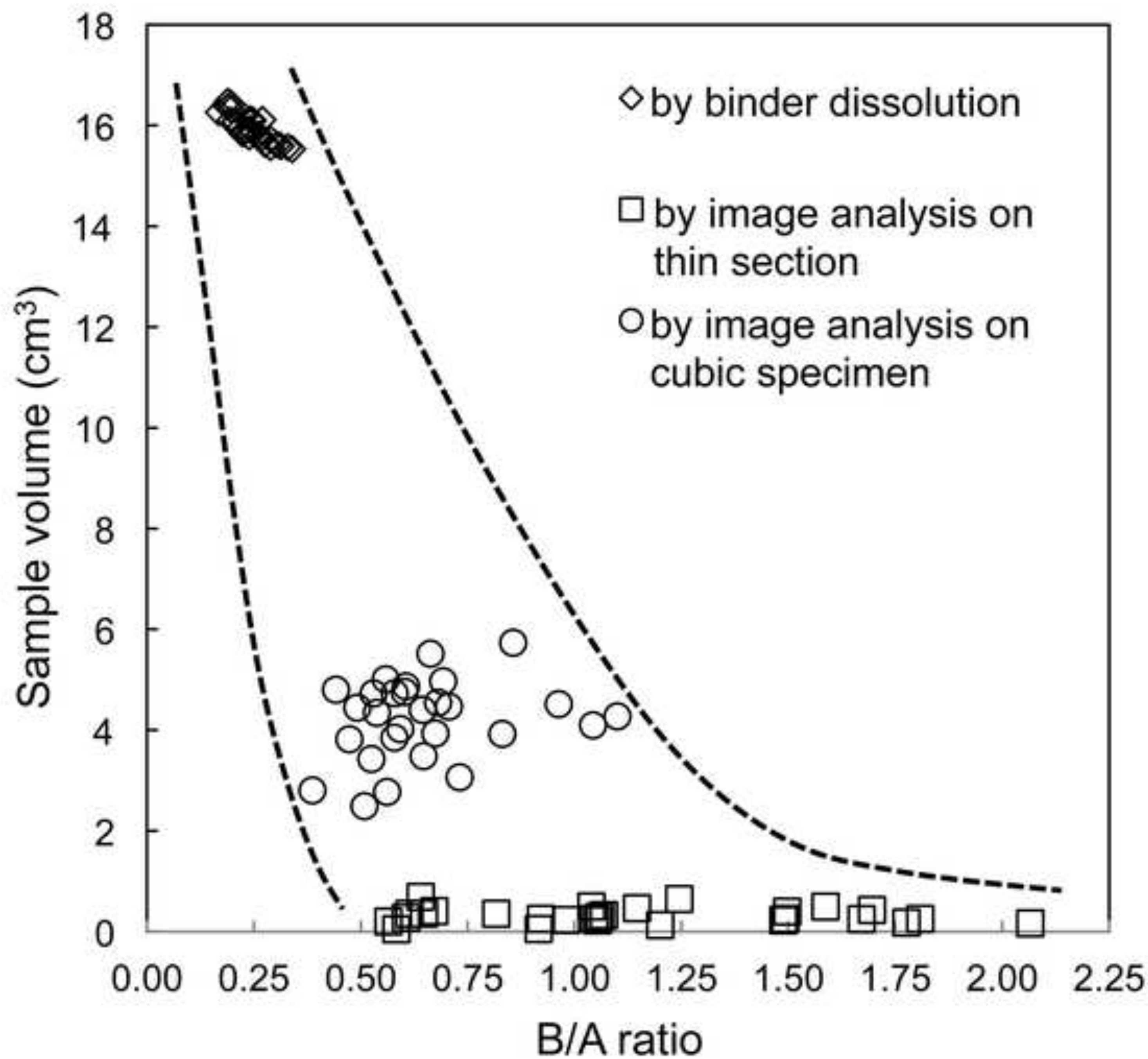
18
16
14
12
10
8
6
4
2
0
Sample volume (cm3)
0.00
0.25
0.50
0.75
1.00
1.25
1.50
1.75
2.00
2.25
B/A ratio
by binder dissolution
by image analysis on thin section
by image analysis on cubic specimen

Figure 7

Click here to download Figure Figure 7.tif

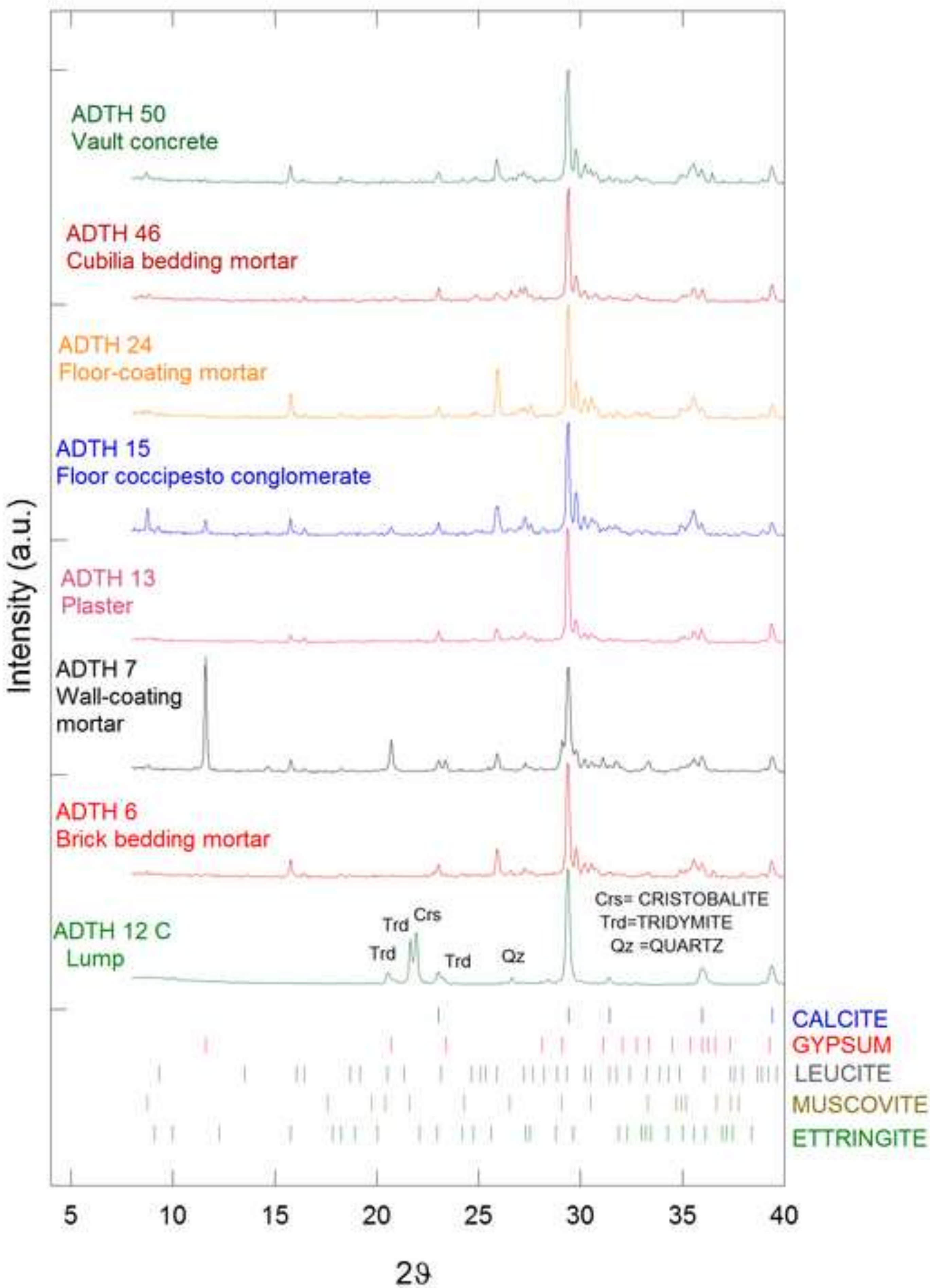

Figure 8a

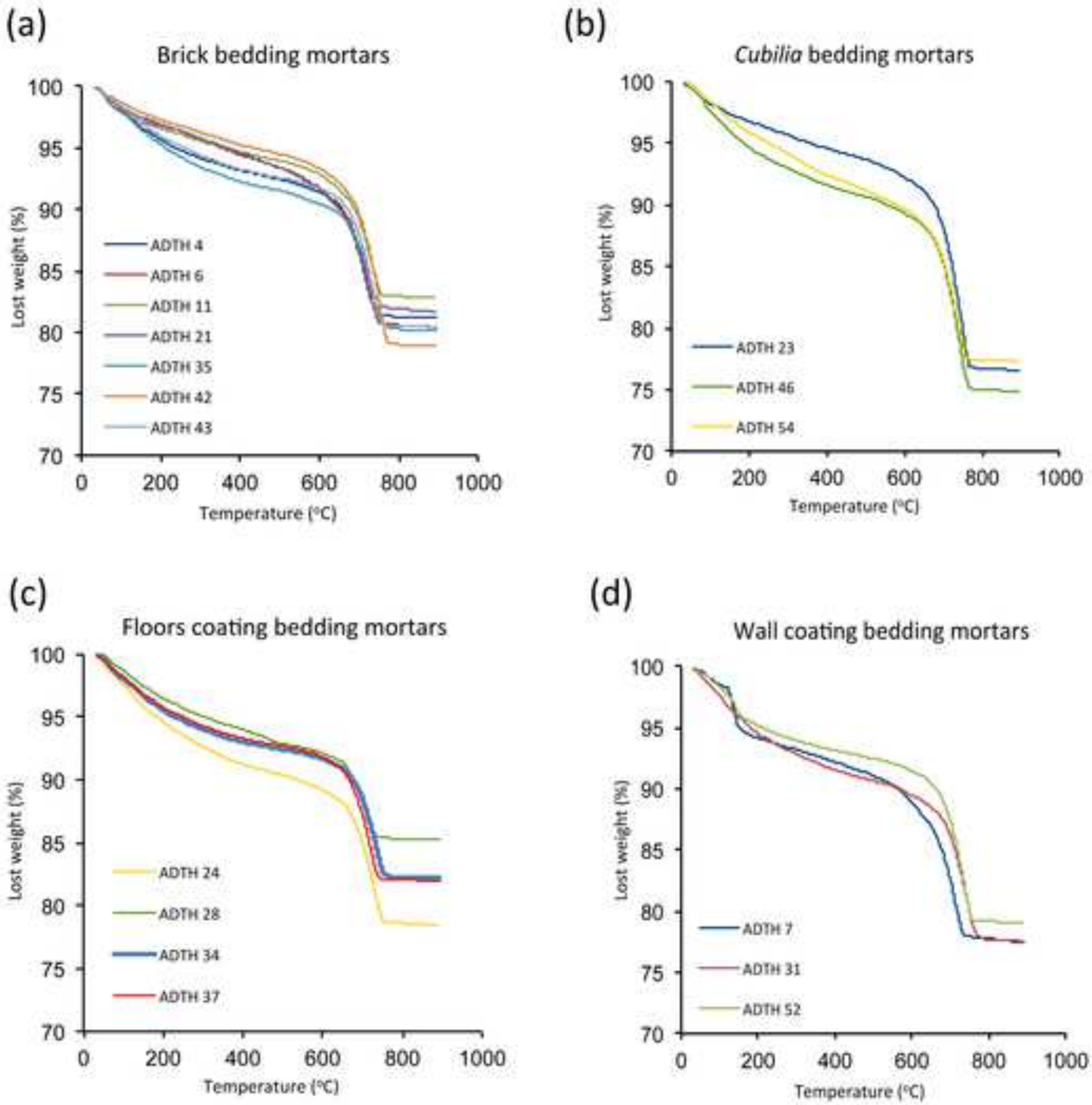
(a)
Brick bedding mortars
Lost weight (%)
Temperature (°C)
ADTH 4
ADTH 6
ADTH 11
ADTH 21
ADTH 35
ADTH 42
ADTH 43
(b)
Cubilia bedding mortars
Lost weight (%)
Temperature (°C)
ADTH 23
ADTH 46
ADTH 54
(c)
Floors coating bedding mortars
Lost weight (%)
Temperature (°C)
ADTH 24
ADTH 28
ADTH 34
ADTH 37
(d)
Wall coating bedding mortars
Lost weight (%)
Temperature (°C)
ADTH 7
ADTH 31
ADTH 52

Figure 8b

Click here to download Figure Figure 8b.tif

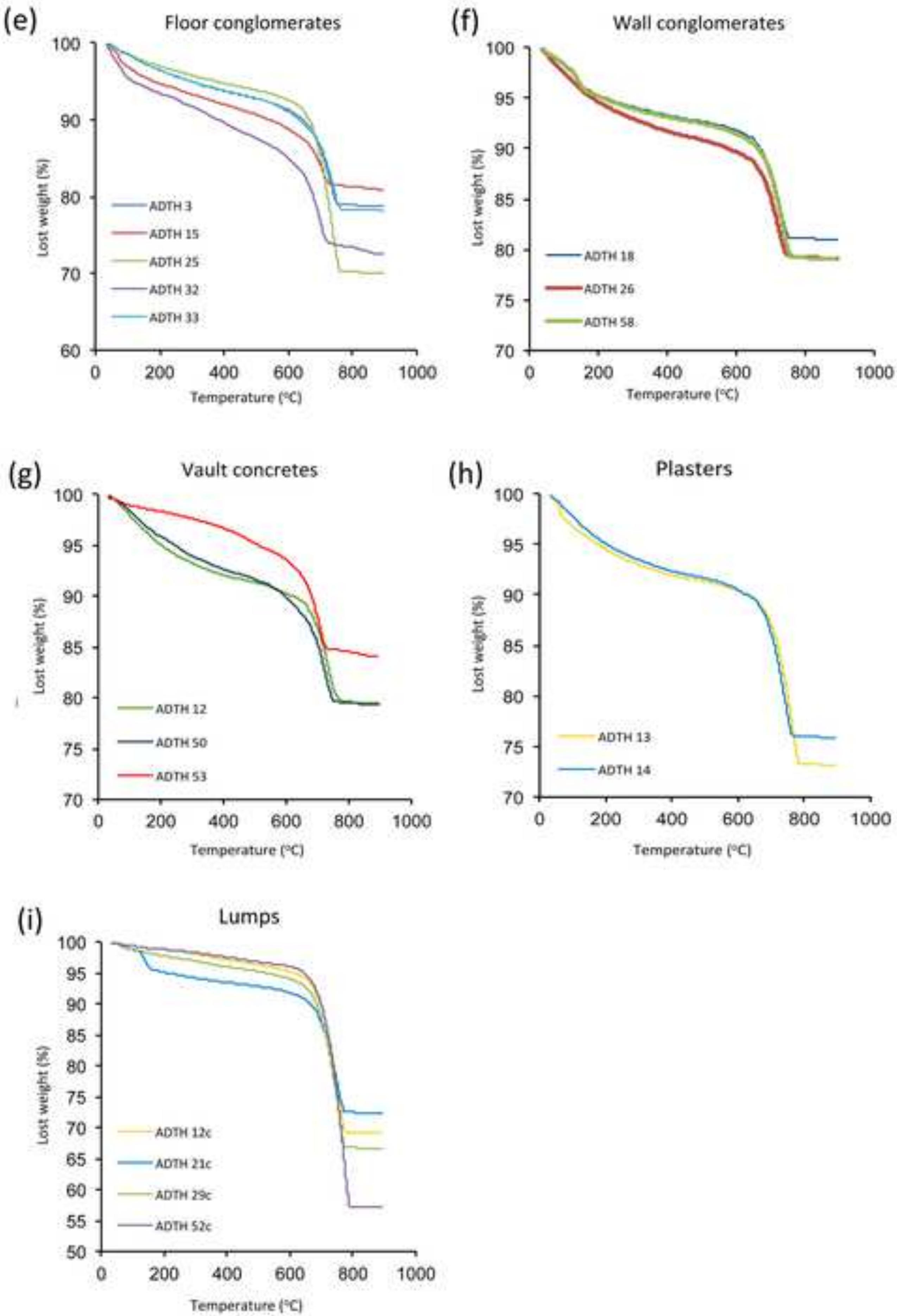

Figure 9

Click here to download Figure Figure 9.tif

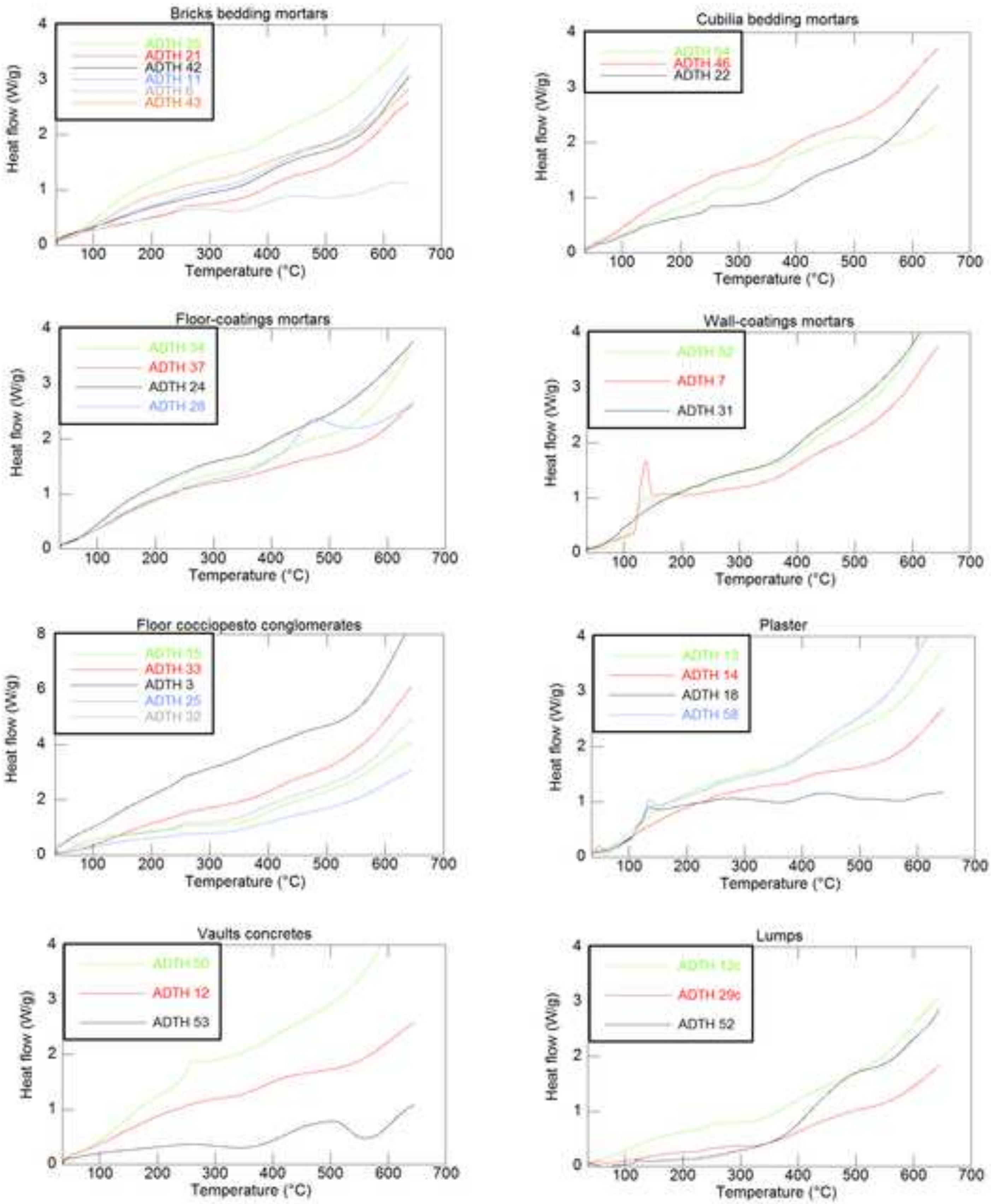

Figure 10

Click here to download Figure Figure 10.tif

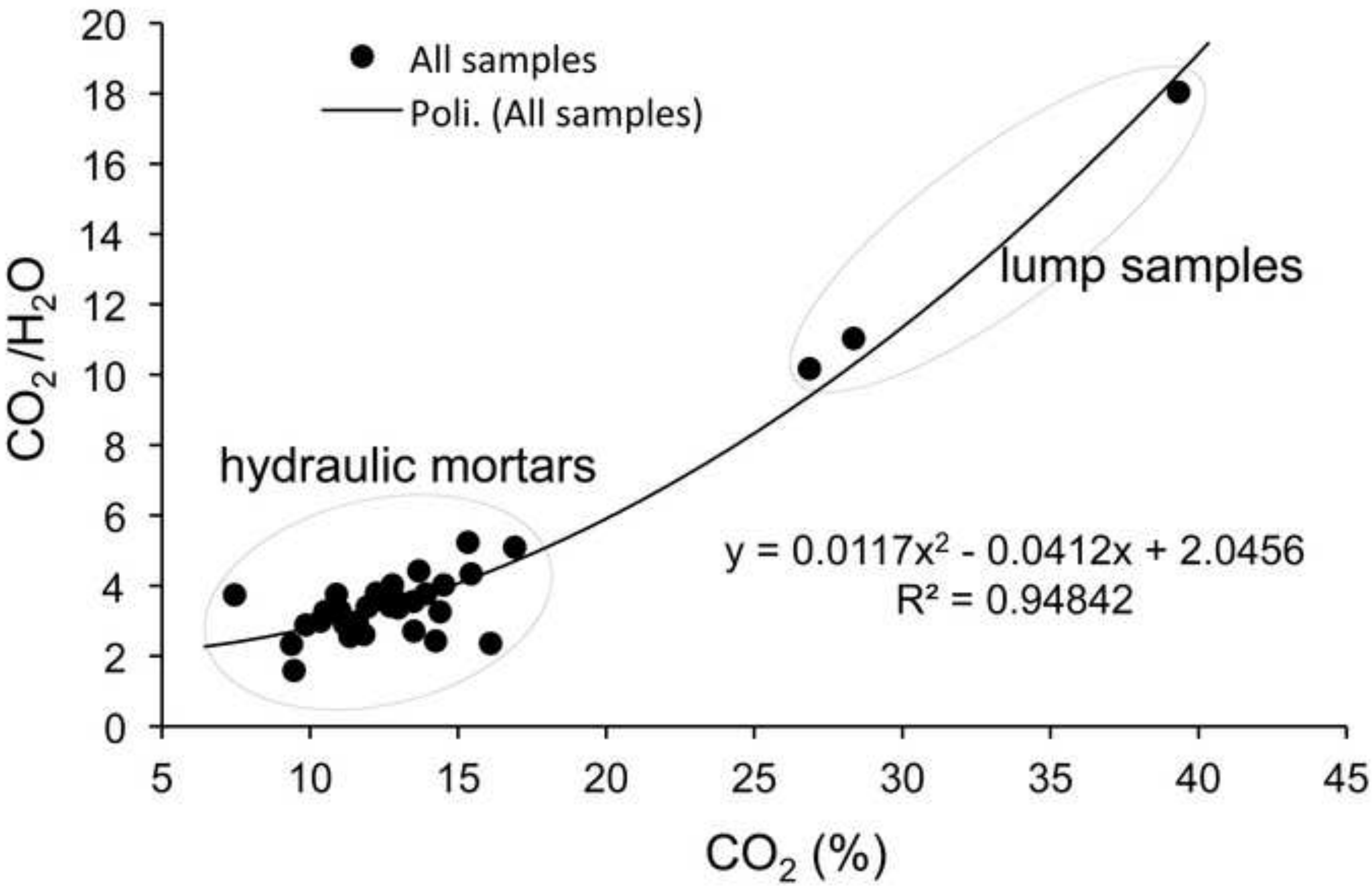

Figure 11

Click here to download Figure Figure 11.tif

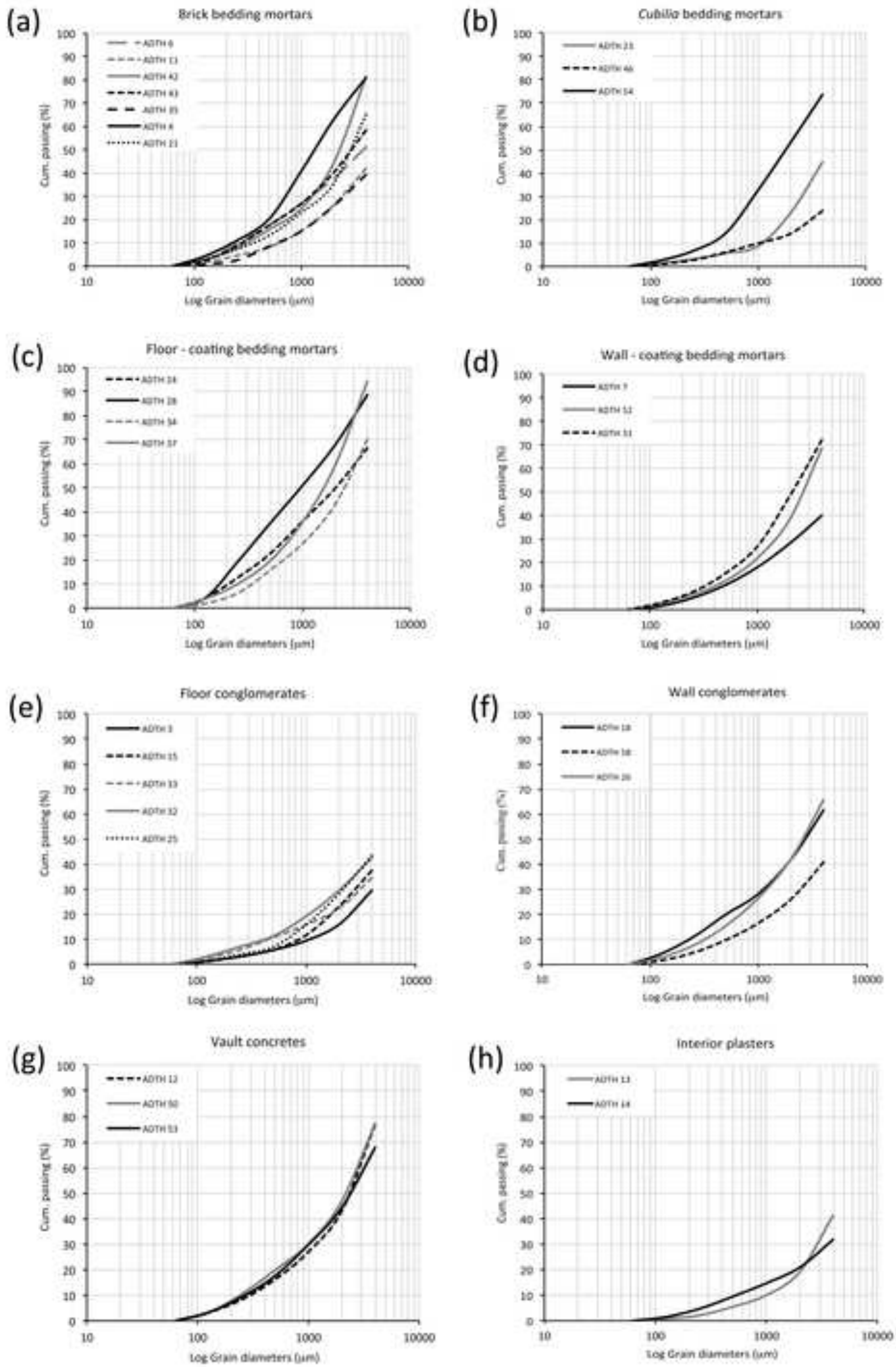

Figure 12a,b

Click here to download Figure Figure 12a,b.tif

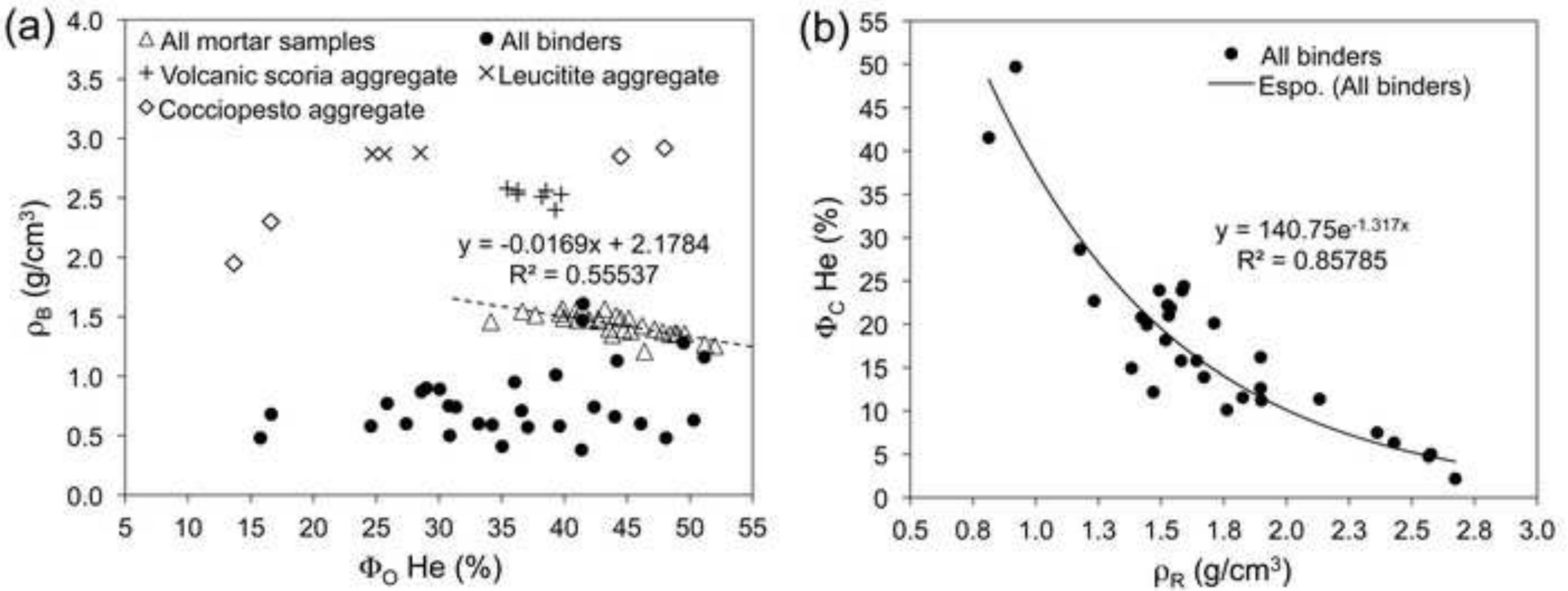

Figure 13a,b

Click here to download Figure Figure 13a,b.tif

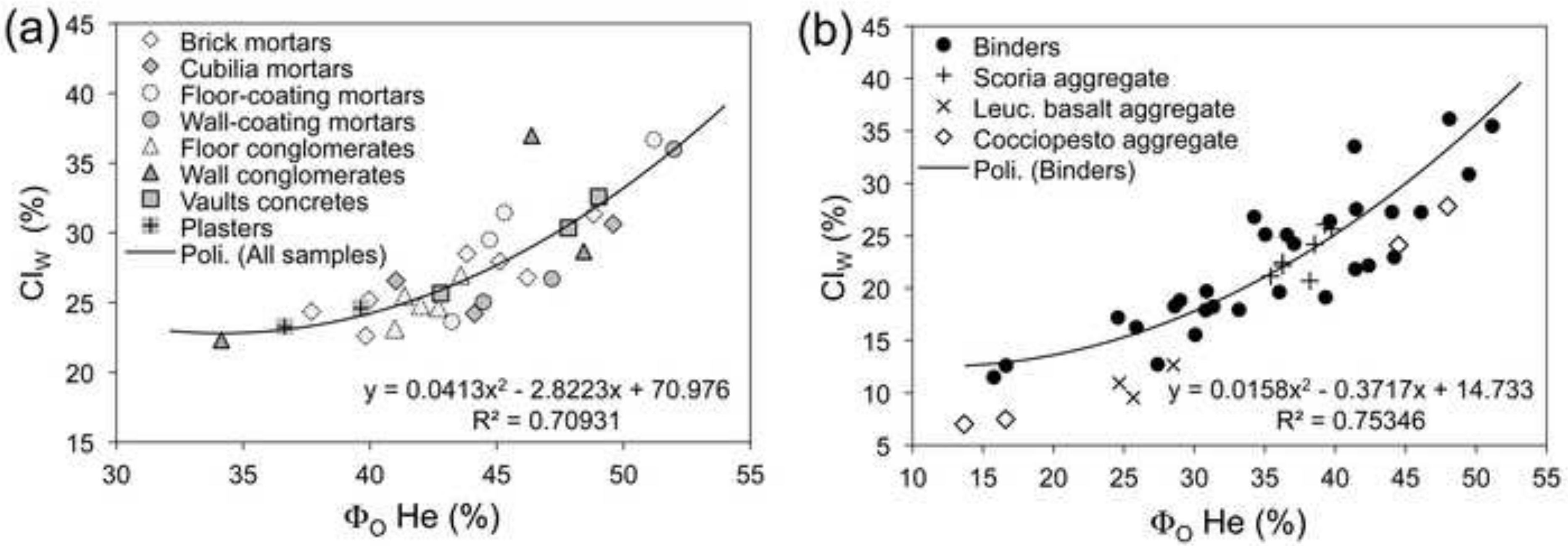

Figure 14

Click here to download Figure Figure 14.tif

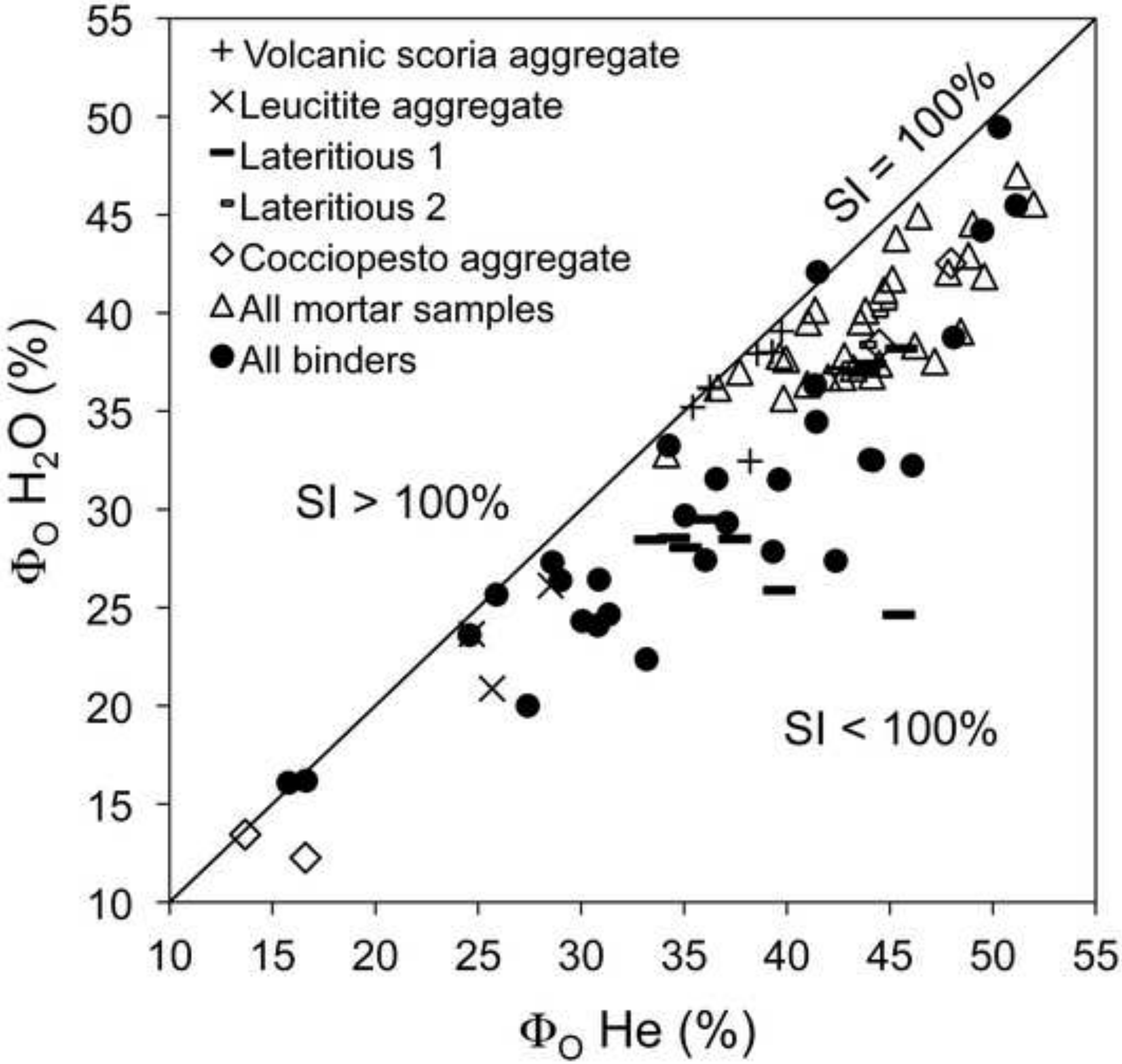

Figure 15

Click here to download Figure Figure 15.tif

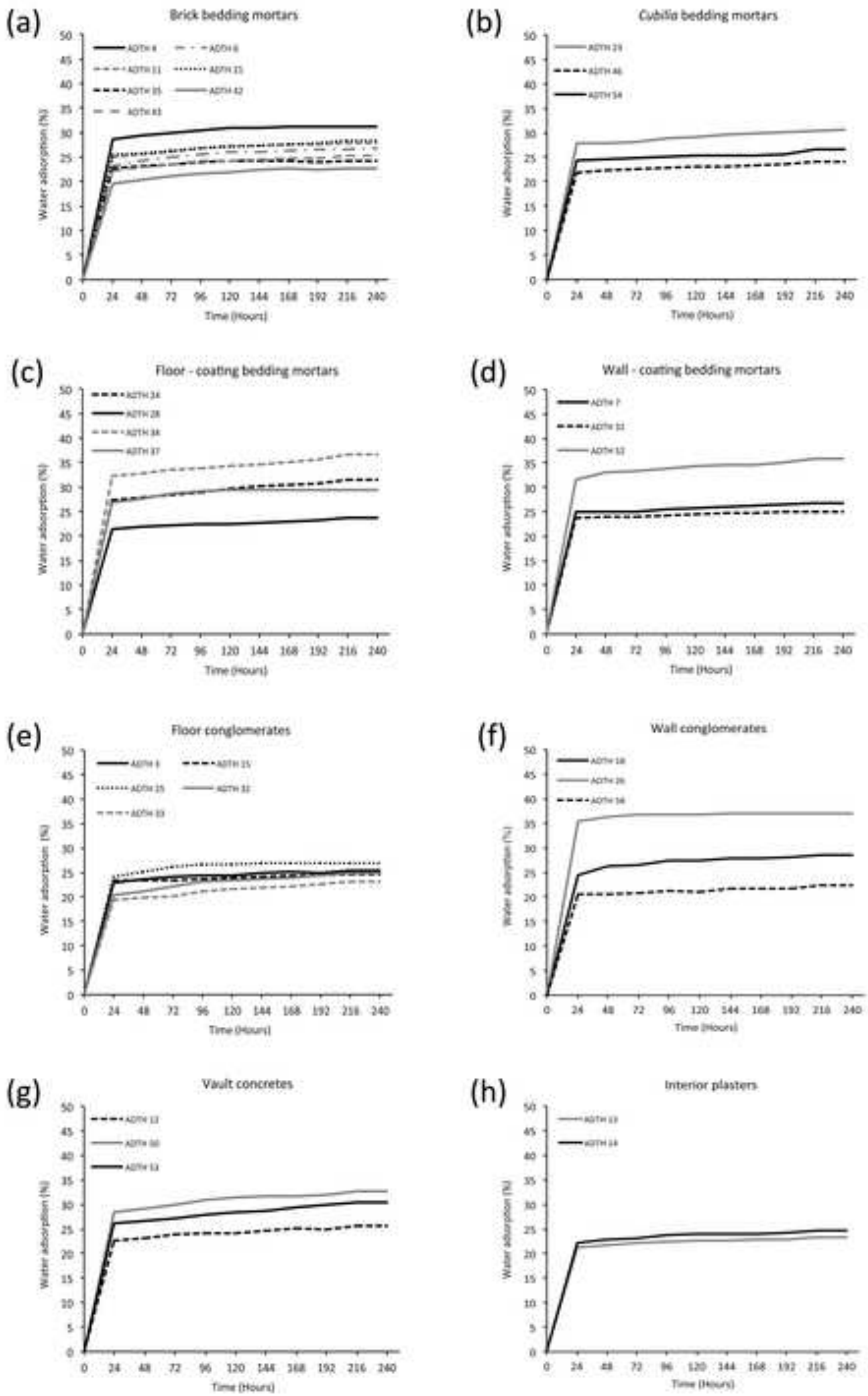

Figure 16a,b,c

Click here to download Figure Figure 16.tif

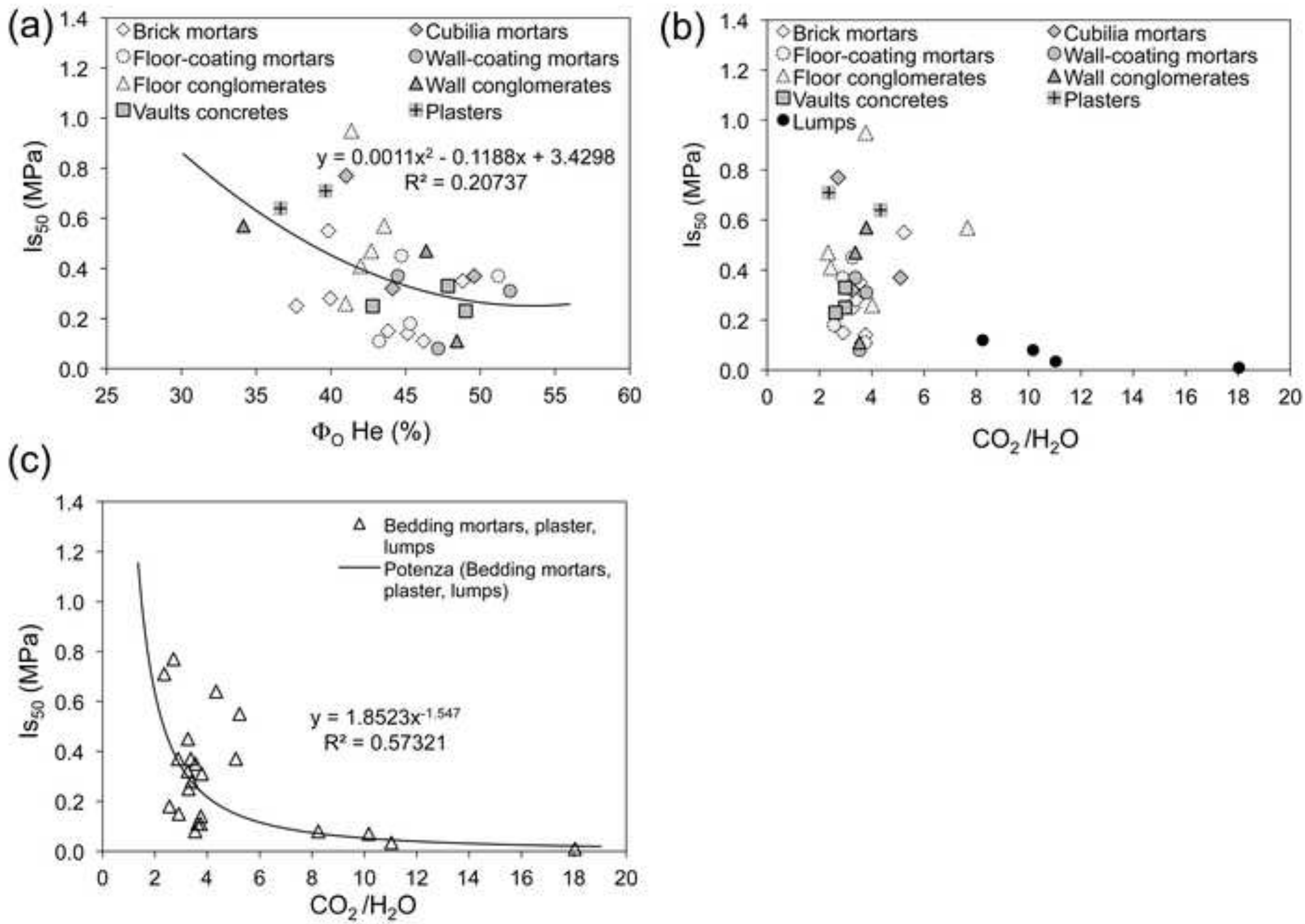

Table 1

Mortar typology	Sample	Room of baths	Height (cm)	Fragments				Crystal-clasts		
				Scoria	Leucitite	*Coccio-pesto*	Marble	Cpx	Hnb	Bt
Brick bedding mortars	ADTH 4	*Calidarium*	-98	99.5	0	0	0.5	0	0	0
	ADTH 6	*Calidarium*	-35	99.1	0.7	0	0.2	0	0	0
	ADTH 11	*Fire room*	-85	98.2	1.5	0	0	0.3	0	0
	ADTH 21	*Natatio*	90	99.8	0	0	0.2	0	0	0
	ADTH 35	*Sudatio*	-16	94.3	3.8	0	0	1.9	0	0
	ADTH 42	*Sudatio*	-98	96.8	1.1	0	0.1	0.9	1.1	0
	ADTH 43	*Sudatio*	7	99.4	0	0	0.6	0	0	0
Cubilia bedding mortars	ADTH 23	*Natatio*	58	99.9	0	0	0.1	0	0	0
	ADTH 46	*Sudatio*	-23	97.8	0.8	0	0.2	1.2	0	0
	ADTH 54	*Apodyterium*	107	95.7	2.1	0	0.3	1.2	0.7	0
Floor-coating bedding mortars	ADTH 24	*Natatio*	-25	95.4	0	4.3	0	0	0.3	0
	ADTH 28	*Natatio*	-138	87.9	1.0	5.1	0	1.0	4.0	1.0
	ADTH 34	*Sudatio*	-4	95.2	0	4.8	0	0	0	0
	ADTH 37	*Laconicum*	-64	95.1	0	4.5	0	0.4	0	0
Wall-coating mortars	ADTH 7	*Calidarium*	28	98.0	0	0	0	1.0	1.0	0
	ADTH 31	*Laconicum*	25	98.3	0.8	0	0	0	0.9	0
	ADTH 52	*Apodyterium*	20	99.3	0	0	0	0.7	0	0
Floor conglomer. *(rudus)*	ADTH 3	*Calidarium*	-10	85.7	0	13.8	0	0.5	0	0
	ADTH 15	*Tepidarium*	-12	87.9	0	12.1	0	0	0	0
	ADTH 25	*Natatio*	-28	79.8	3.2	15.2	0	1.8	0	0
	ADTH 32	*Laconicum*	-7	78.7	5.1	16.2	0	0	0	0
	ADTH 33	*Laconicum*	-5	81.0	2.1	15.3	0	0	1.6	0
Wall conglomer. *(trullisatio)*	ADTH 18	*Frigidarium*	30	73.1	7.7	17.7	0	0.9	0.6	0
	ADTH 26	*Natatio*	-109	76.5	2.7	20.4	0	0	0.4	0
	ADTH 58	*Apodyterium*	26	85.1	1.1	13.8	0	0	0	0
Vault concretes	ADTH 12	*Calidarium*	0	98.5	0.9	0	0.1	0	0.5	0
	ADTH 50	*Apodyterium*	52	98.7	0	0	0.1	1.2	0	0
	ADTH 53	*Apodyterium*	58	99.8	0	0	0.2	0	0	0
Plasters	ADTH 13	*Tepidarium*	-7	84.4	5.2	8.2	0	0	2.2	0
	ADTH 14	*Calidarium*	40	81.7	0	16.6	0	1.4	0.3	0

Table 2

Sample	Mortar tipology	Circularity variation range (min - max)	Average circularity	Mean of average circularity	Standard deviation	Variation coefficient
ADTH 4	Brick bedding mortars	0,02 - 0,99	0.67	0.57	0.07	0.12
ADTH 6		0,08- 0,99	0.57			
ADTH 11		0,04 - 1	0.50			
ADTH 21		0,05 - 0,96	0.45			
ADTH 35		0,01 - 0,99	0.59			
ADTH 42		0,05 - 0,99	0.61			
ADTH 43		0,06 - 0,98	0.58			
ADTH 54	*Cubilia* bedding mortars	0,01 - 1	0.64	0.59	0.05	0.09
ADTH 46		0,04 - 1	0.58			
ADTH 23		0,03 - 1	0.54			
ADTH 24	Floors-coating beding mortars	0,04 - 0,98	0.53	0.54	0.04	0.07
ADTH 28		0,05 - 1	0.48			
ADTH 34		0,03 - 1	0.56			
ADTH 37		0,01 - 1	0.58			
ADTH 7	Wall-coating bedding mortars	0,03 - 1	0.64	0.52	0.11	0.21
ADTH 31		0,04 - 0,99	0.45			
ADTH 52		0,01 - 0,99	0.46			
ADTH 3	Floor cocciopesto conglomerates (*rudus*)	0,03 - 0,99	0.58	0.54	0.04	0.07
ADTH 15		0,03 - 0,99	0.50			
ADTH 25		0,07 - 0,99	0.52			
ADTH 32		0,02 - 1	0.52			
ADTH 33		0,02 - 1	0.59			
ADTH 18	Wall cocciopesto conglomerates (*trullisatio*)	0,01 - 1	0.58	0.59	0.02	0.04
ADTH 26		0,06 - 0,99	0.61			
ADTH 58		0,01 - 0,97	0.57			
ADTH 12	Vault concretes	0,03 - 0,99	0.59	0.58	0.02	0.03
ADTH 50		0,02 - 0,99	0.56			
ADTH 53		0,04 - 1	0.59			
ADTH 13	Plasters	0,04 - 1	0.56	0.57	0.01	0.02
ADTH 14		0,02 - 0,97	0.58			

Table 3

Mortar tipology	Sample	by image analysis on cube specimens (vol.%)			by image analysis on thin section (vol.%)			by binder dissolution method (vol.%)		
		Aggregate	Binder	B / A	Aggregate	Binder	B / A	Aggregate	Binder	B / A
Brick bedding mortars	ADTH 4	63.31	36.69	0.58	63.15	36.85	0.58	76.64	23.36	0.32
	ADTH 6	65.37	34.63	0.53	55.04	44.96	0.82	76.15	23.85	0.33
	ADTH 11	48.95	51.05	1.04	63.90	36.10	0.56	82.05	17.95	0.23
	ADTH 21	59.08	40.92	0.69	60.68	39.32	0.65	78.82	21.18	0.28
	ADTH 35	72.09	27.91	0.39	61.95	38.05	0.61	81.30	18.70	0.24
	ADTH 42	50.95	49.06	0.96	40.19	59.81	1.49	80.06	19.94	0.26
	ADTH 43	60.14	39.86	0.66	52.05	47.95	0.92	79.42	20.58	0.27
Cubilia bedding mortars	ADTH 54	60.73	39.27	0.65	48.69	51.31	1.05	83.66	16.34	0.35
	ADTH 46	57.77	42.23	0.73	48.35	51.65	1.07	77.50	22.50	0.30
	ADTH 23	67.04	32.96	0.49	48.87	51.13	1.05	74.66	25.34	0.21
Floor-coating bedding mortars	ADTH 24	63.35	36.65	0.58	46.60	53.40	1.15	81.71	18.29	0.23
	ADTH 28	69.35	30.65	0.44	44.55	55.45	1.24	80.69	19.31	0.24
	ADTH 34	65.04	34.96	0.54	35.61	64.39	1.81	77.57	22.43	0.29
	ADTH 37	47.62	52.38	1.10	37.10	62.90	1.70	78.36	21.64	0.28
Wall-coating mortars	ADTH 7	59.50	40.50	0.68	38.66	61.34	1.59	75.22	24.78	0.33
	ADTH 31	54.62	45.39	0.83	40.12	59.88	1.49	79.22	20.78	0.26
	ADTH 52	60.80	39.20	0.64	40.04	59.96	1.50	80.38	19.62	0.25
Floor conglomerates *(rudus)*	ADTH 3	66.29	33.71	0.51	62.27	37.73	0.61	80.16	19.84	0.25
	ADTH 15	58.62	41.39	0.71	59.81	40.19	0.67	80.53	19.47	0.24
	ADTH 25	65.60	34.40	0.52	45.46	54.54	1.20	84.12	15.88	0.19
	ADTH 32	62.41	37.60	0.60	50.50	49.50	0.98	81.51	18.49	0.23
	ADTH 33	62.27	37.73	0.61	48.55	51.45	1.06	83.57	16.43	0.20
Wall conglomerates *(trullisatio)*	ADTH 18	59.73	40.27	0.67	49.03	50.97	1.04	83.51	16.49	0.20
	ADTH 26	53.87	46.13	0.86	52.19	47.81	0.92	84.12	15.88	0.19
	ADTH 58	64.17	35.83	0.56	60.97	39.03	0.64	78.76	21.24	0.27
Vault concretes	ADTH 12	62.80	37.20	0.59	36.02	63.98	1.78	80.58	19.42	0.25
	ADTH 50	67.87	32.13	0.47	32.62	67.38	2.07	85.60	14.40	0.18
	ADTH 53	64.05	35.96	0.56	37.44	62.56	1.67	82.81	17.19	0.22
Plasters	ADTH 13	60.48	39.52	0.65	53.40	46.60	0.87	81.68	18.32	0.22
	ADTH 14	61.49	38.51	0.63	49.39	50.61	1.02	80.01	19.99	0.25

Table 4

Sample	A	B	B / A (wt)	A	B	Aggregate fragment / crystal weights (g)								B (g)	Aggregate fragment / crystal volumes (cm^3)								B (cm^3)	B / A (vol)	B	A
	wt (g)			wt (%)		Sc	Le	CP	Mbl	Cpx	Hnb	Bt	Total		Sc	Le	CP	Mbl	Cpx	Hnb	Bt	Total			vol (%)	
ADTH 4	22.55	7.45	0.33	75.17	24.83	22.44	0.00	0.00	0.11	0.00	0.00	0.00	22.55	7.45	8.98	0.00	0.00	0.04	0.00	0.00	0.00	9.02	2.75	0.30	23.36	76.64
ADTH 6	22.39	7.61	0.34	74.63	25.37	22.19	0.16	0.00	0.04	0.00	0.00	0.00	22.39	7.61	8.87	0.07	0.00	0.02	0.00	0.00	0.00	8.97	2.81	0.31	23.85	76.15
ADTH 11	24.24	5.76	0.24	80.80	19.20	23.80	0.36	0.00	0.00	0.07	0.00	0.00	24.24	5.76	9.52	0.17	0.00	0.00	0.02	0.00	0.00	9.72	2.13	0.22	17.95	82.05
ADTH 21	23.24	6.77	0.29	77.45	22.55	23.19	0.00	0.00	0.05	0.00	0.00	0.00	23.24	6.77	9.28	0.00	0.00	0.02	0.00	0.00	0.00	9.29	2.50	0.27	21.18	78.82
ADTH 35	24.00	6.00	0.25	80.01	19.99	22.63	0.91	0.00	0.00	0.46	0.00	0.00	24.00	6.00	9.05	0.43	0.00	0.00	0.13	0.00	0.00	9.62	2.21	0.23	18.70	81.30
ADTH 42	23.64	6.36	0.27	78.79	21.21	22.88	0.26	0.00	0.02	0.21	0.26	0.00	23.64	6.36	9.15	0.12	0.00	0.01	0.06	0.08	0.00	9.43	2.35	0.25	19.94	80.06
ADTH 43	23.42	6.58	0.28	78.08	21.92	23.28	0.00	0.00	0.14	0.00	0.00	0.00	23.42	6.58	9.31	0.00	0.00	0.05	0.00	0.00	0.00	9.37	2.43	0.26	20.58	79.42
ADTH 23	24.76	5.24	0.21	82.53	17.47	24.73	0.00	0.00	0.02	0.00	0.00	0.00	24.76	5.24	9.89	0.00	0.00	0.01	0.00	0.00	0.00	9.90	1.93	0.20	16.34	83.66
ADTH 46	22.83	7.17	0.31	76.10	23.90	22.33	0.18	0.00	0.05	0.27	0.00	0.00	22.83	7.17	8.93	0.09	0.00	0.02	0.08	0.00	0.00	9.12	2.65	0.29	22.50	77.50
ADTH 54	21.94	8.06	0.37	73.12	26.88	20.99	0.46	0.00	0.07	0.26	0.15	0.00	21.94	8.06	8.40	0.22	0.00	0.02	0.08	0.05	0.00	8.77	2.98	0.34	25.34	74.66
ADTH 24	24.12	5.88	0.24	80.41	19.59	23.01	0.00	1.04	0.00	0.00	0.07	0.00	24.12	5.88	9.21	0.00	0.46	0.00	0.00	0.02	0.00	9.69	2.17	0.22	18.29	81.71
ADTH 28	23.84	6.16	0.26	79.48	20.52	20.96	0.24	1.22	0.00	0.24	0.95	0.24	23.84	6.16	8.38	0.11	0.54	0.00	0.07	0.30	0.08	9.49	2.27	0.24	19.31	80.69
ADTH 34	22.81	7.19	0.32	76.03	23.97	21.71	0.00	1.09	0.00	0.00	0.00	0.00	22.81	7.19	8.69	0.00	0.49	0.00	0.00	0.00	0.00	9.17	2.65	0.29	22.43	77.57
ADTH 37	23.07	6.93	0.30	76.89	23.11	21.94	0.00	1.04	0.00	0.09	0.00	0.00	23.07	6.93	8.77	0.00	0.46	0.00	0.03	0.00	0.00	9.27	2.56	0.28	21.64	78.36
ADTH 7	22.13	7.87	0.36	73.78	26.22	21.69	0.00	0.00	0.00	0.22	0.22	0.00	22.13	7.87	8.68	0.00	0.00	0.00	0.07	0.07	0.00	8.81	2.90	0.33	24.78	75.22
ADTH 31	23.36	6.64	0.28	77.87	22.13	22.96	0.19	0.00	0.00	0.00	0.21	0.00	23.36	6.64	9.19	0.09	0.00	0.00	0.00	0.07	0.00	9.34	2.45	0.26	20.78	79.22
ADTH 52	23.73	6.27	0.26	79.11	20.89	23.57	0.00	0.00	0.00	0.17	0.00	0.00	23.73	6.27	9.43	0.00	0.00	0.00	0.05	0.00	0.00	9.48	2.31	0.24	19.62	80.38
ADTH 3	23.58	6.42	0.27	78.60	21.40	20.21	0.00	3.25	0.00	0.12	0.00	0.00	23.58	6.42	8.08	0.00	1.45	0.00	0.03	0.00	0.00	9.57	2.37	0.25	19.84	80.16
ADTH 15	23.70	6.30	0.27	79.00	21.00	20.83	0.00	2.87	0.00	0.00	0.00	0.00	23.70	6.30	8.33	0.00	1.28	0.00	0.00	0.00	0.00	9.61	2.32	0.24	19.47	80.53
ADTH 25	24.83	5.18	0.21	82.75	17.25	19.81	0.79	3.77	0.00	0.45	0.00	0.00	24.83	5.18	7.92	0.38	1.68	0.00	0.13	0.00	0.00	10.12	1.91	0.19	15.88	84.12
ADTH 32	23.94	6.06	0.25	79.81	20.19	18.84	1.22	3.88	0.00	0.00	0.00	0.00	23.94	6.06	7.54	0.58	1.73	0.00	0.00	0.00	0.00	9.85	2.24	0.23	18.49	81.51
ADTH 33	24.65	5.35	0.22	82.17	17.83	19.97	0.52	3.77	0.00	0.00	0.39	0.00	24.65	5.35	7.99	0.25	1.68	0.00	0.00	0.13	0.00	10.04	1.97	0.20	16.43	83.57
ADTH 18	24.57	5.43	0.22	81.91	18.09	17.96	1.89	4.35	0.00	0.22	0.15	0.00	24.57	5.43	7.19	0.90	1.94	0.00	0.07	0.05	0.00	10.14	2.00	0.20	16.49	83.51
ADTH 26	24.79	5.21	0.21	82.62	17.38	18.96	0.67	5.06	0.00	0.00	0.10	0.00	24.79	5.21	7.58	0.32	2.26	0.00	0.00	0.03	0.00	10.19	1.92	0.19	15.88	84.12
ADTH 58	23.12	6.88	0.30	77.06	22.94	19.67	0.25	3.19	0.00	0.00	0.00	0.00	23.12	6.88	7.87	0.12	1.42	0.00	0.00	0.00	0.00	9.41	2.54	0.27	21.24	78.76
ADTH 12	23.78	6.22	0.26	79.28	20.72	23.43	0.21	0.00	0.02	0.00	0.12	0.00	23.78	6.22	9.37	0.10	0.00	0.01	0.00	0.04	0.00	9.52	2.29	0.24	19.42	80.58
ADTH 50	25.39	4.61	0.18	84.62	15.38	25.06	0.00	0.00	0.03	0.30	0.00	0.00	25.39	4.61	10.02	0.00	0.00	0.01	0.09	0.00	0.00	10.12	1.70	0.17	14.40	85.60
ADTH 53	24.49	5.51	0.23	81.63	18.37	24.44	0.00	0.00	0.05	0.00	0.00	0.00	24.49	5.51	9.78	0.00	0.00	0.02	0.00	0.00	0.00	9.79	2.03	0.21	17.19	82.81
ADTH 13	24.06	5.94	0.25	80.21	19.79	20.31	1.25	1.97	0.00	0.00	0.53	0.00	24.06	5.94	8.12	0.60	0.88	0.00	0.00	0.17	0.00	9.77	2.19	0.22	18.32	81.68
ADTH 14	23.53	6.47	0.27	78.44	21.56	19.23	0.00	3.91	0.00	0.33	0.07	0.00	23.53	6.47	7.69	0.00	1.74	0.00	0.10	0.02	0.00	9.55	2.39	0.25	19.99	80.01

Table 5

		AGGREGATE DATA (by volume)				
Mortar tipology	Sample	by specimen image analysis	by thin section image analysis	by binder dissolution method	Mortar thickness	Vitruvio's values
		vol%	vol%	vol%	cm	vol%
Brick bedding mortars	ADTH 4	63.31	63.15	76.64	1.5-2	65-70
	ADTH 6	65.37	55.04	76.15		
	ADTH 11	48.95	63.9	82.05		
	ADTH 21	59.08	60.68	78.82		
	ADTH 35	72.09	61.95	81.30		
	ADTH 42	50.95	40.19	80.06		
	ADTH 43	60.14	52.05	79.42		
Cubilia bedding mortars	ADTH 23	67.04	48.87	83.66	1.5-2.5	65-70
	ADTH 46	57.77	48.35	77.50		
	ADTH 54	60.73	48.69	74.66		
Floor-coating bedding mortars	ADTH 24	63.35	46.6	81.71	3.5-6	70-80
	ADTH 28	69.35	44.55	80.69		
	ADTH 34	65.04	35.61	77.57		
	ADTH 37	47.62	37.1	78.36		
Wall-coating mortars	ADTH 7	59.50	38.66	75.22	1.5-3	70-80
	ADTH 31	54.62	40.12	79.22		
	ADTH 52	60.80	40.04	80.38		
Floor conglomerates *(rudus)*	ADTH 3	66.29	62.27	80.16	12.5-20	70-80
	ADTH 15	58.62	59.81	80.53		
	ADTH 25	65.60	45.46	84.12		
	ADTH 32	62.41	50.5	81.51		
	ADTH 33	62.27	48.55	83.57		
Wall conglomerates (trullisatio)	ADTH 18	59.73	49.03	83.51	2.5-5	70-80
	ADTH 26	53.87	52.19	84.12		
	ADTH 58	64.17	60.97	78.76		
Vault concretes	ADTH 12	62.80	36.02	80.58	>20	70-80
	ADTH 50	67.87	32.62	85.60		
	ADTH 53	64.05	37.44	82.81		
Plasters	ADTH 13	60.48	53.4	81.68	1.5-2.5	65-70
	ADTH 14	61.49	49.39	80.01		

Table 6

Sample	Binder / aggregate ratio (by volume)			Specimen volume (cm^3)		
	by cubic specimen image analysis	by thin section image analysis	by dissolution binder	cubic specimen	thin section	dissolution sample
ADTH 4	0.58	0.58	0.30	4.73	0.05	15.62
ADTH 6	0.53	0.82	0.31	4.73	0.35	15.59
ADTH 11	1.04	0.56	0.22	4.09	0.20	15.96
ADTH 21	0.69	0.65	0.27	4.97	0.35	15.76
ADTH 35	0.39	0.61	0.23	2.80	0.35	15.92
ADTH 42	0.96	1.49	0.25	4.51	0.22	15.85
ADTH 43	0.66	0.92	0.26	5.51	0.25	15.80
ADTH 23	0.49	1.05	0.20	4.44	0.25	16.10
ADTH 46	0.73	1.07	0.29	3.06	0.33	15.71
ADTH 54	0.65	1.05	0.34	3.48	0.22	15.53
ADTH 24	0.58	1.15	0.22	3.85	0.46	15.84
ADTH 28	0.44	1.24	0.24	4.80	0.65	15.78
ADTH 34	0.54	1.81	0.29	4.34	0.25	15.57
ADTH 37	1.10	1.70	0.28	4.27	0.43	15.63
ADTH 7	0.68	1.59	0.33	4.54	0.49	15.57
ADTH 31	0.83	1.49	0.26	3.92	0.25	15.82
ADTH 52	0.64	1.50	0.24	4.40	0.40	15.90
ADTH 3	0.51	0.61	0.25	2.49	0.28	16.10
ADTH 15	0.71	0.67	0.24	4.46	0.41	16.12
ADTH 25	0.52	1.20	0.19	3.42	0.13	16.37
ADTH 32	0.60	0.98	0.23	4.76	0.23	16.18
ADTH 33	0.61	1.06	0.20	4.87	0.29	16.32
ADTH 18	0.67	1.04	0.20	3.93	0.50	16.42
ADTH 26	0.86	0.92	0.19	5.73	0.05	16.47
ADTH 58	0.56	0.64	0.27	5.01	0.69	16.11
ADTH 12	0.59	1.78	0.24	4.02	0.18	15.93
ADTH 50	0.47	2.07	0.17	3.82	0.17	16.26
ADTH 53	0.56	1.67	0.21	2.77	0.25	16.07
ADTH 13	0.65	0.87	0.22	5.77	0.65	16.32
ADTH 14	0.63	1.02	0.25	5.92	0.12	16.20

Table 7

Samples tipology	Δ (25-120°C)	Δ (120-200°C)	Δ (200-400°C)	Δ (400-600°C)	Δ (600-850°C)
ADTH 43	2.3	1.7	2.8	1.6	11.1
ADTH 6	2.5	0.9	2.2	2.8	11.1
ADTH 11	2.1	1.2	2.2	1.7	10.9
ADTH 42	1.7	1	2.1	1.9	14.4
ADTH 21	2.1	0.9	2.5	2.9	9.8
ADTH 4	2.5	1.9	2.4	1.8	10.2
ADTH 35	2.5	2.3	3	1.8	10.3
ADTH 54	2.3	1.8	3.5	2.7	12.4
ADTH 46	4	1.4	3	2.3	14.4
ADTH 22	2.1	1.1	2.2	2.4	15.6
ADTH 34	2.6	1.9	2.5	1.3	9.5
ADTH 37	2.4	1.8	2.5	1.5	9.9
ADTH 24	3.2	2.2	3.4	2.1	10.6
ADTH 28	1.7	1.9	2.4	1.9	6.8
ADTH 15	3.5	1.8	2.7	3.3	7.6
ADTH 33	1.9	1.6	2.6	2.9	12.7
ADTH 3	1.9	1.6	2.7	2.6	12.3
ADTH 25	1.7	1.3	2.2	2.2	21.7
ADTH 32	5	1.5	3.9	4.6	12.2
ADTH 18	2.4	2.3	2	1.5	10.7
ADTH 26	3.1	2.3	2.9	2.1	10.5
ADTH 58	2.3	2.7	1.8	1.8	12.3
ADTH 50	2.2	2	3.2	2.7	10.5
ADTH 12	2.7	2.2	3	1.7	11
ADTH 53	1.7	0	1.6	3.2	9.3
ADTH 52	2.3	2.6	2	1.7	12.3
ADTH 7	1.7	4.2	1.9	3.3	11.3
ADTH 31	3.2	2.3	3	2.1	11.8
ADTH 13	2.9	2.1	2.7	1.8	14.6
ADTH 14	3.5	1.7	2.5	1.5	16.1
ADTH 52c	0.7	0.5	1.3	1.5	38.8
ADTH 12c	0.7	0.5	1.6	2.1	25.9
ADTH 21c	1.5	3.4	1.6	1.7	20.5
ADTH 29c	1.4	0.8	1.8	2	27.4

Table 8

Mortar typology	Samples	Weight loss for temperature range (%) 200 - 520^{O} C (H_2O)	520 - 800^{O} C (CO_2)	CO_2/H_2O
Brick bedding mortars	ADTH 4	3.80	13.49	3.55
	ADTH 6	3.46	12.55	3.63
	ADTH 11	2.90	10.89	3.76
	ADTH 21	3.84	11.17	2.91
	ADTH 35	3.35	11.01	3.29
	ADTH 42	2.93	15.33	5.23
	ADTH 43	3.51	11.93	3.40
Cubilia bedding mortars	ADTH 23	3.32	16.91	5.09
	ADTH 46	4.42	14.39	3.26
	ADTH 54	4.98	13.51	2.71
Floor-coating bedding mortars	ADTH 24	4.44	11.35	2.56
	ADTH 28	1.99	7.45	3.74
	ADTH 34	3.42	9.86	2.88
	ADTH 37	3.22	10.50	3.26
Wall-coating mortars	ADTH 7	3.68	13.00	3.53
	ADTH 31	3.85	12.97	3.37
	ADTH 52	3.23	12.24	3.79
Floor conglomer. *(rudus)*	ADTH 3	3.69	13.91	3.77
	ADTH 15	4.02	9.38	2.33
	ADTH 25	3.09	13.67	4.42
	ADTH 32	5.86	14.24	2.43
	ADTH 33	3.61	14.51	4.02
Wall conglomer *(trullisatio).*	ADTH 18	5.96	9.46	1.59
	ADTH 58	3.18	12.78	4.02
	ADTH 26	3.71	12.71	3.43
Vault concretes	ADTH 12	3.89	11.59	2.98
	ADTH 50	4.52	11.82	2.62
	ADTH 53	3.46	10.35	2.99
Plasters	ADTH 13	3.56	15.44	4.34
	ADTH 14	6.83	16.10	2.36
Lumps	ADTH 12 c	2.64	26.86	10.17
	ADTH 52 c	2.18	39.33	18.04
	ADTH 29 c	2.57	28.35	11.03

Table 9

Samples tipology	Samples	Sieve opening (µm)					
		4000	2000	1000	500	250	125
Briks bedding mortars	ADTH 4	81	62,9	40,8	20,2	10,9	4,2
	ADTH 6	50,9	37,6	26,9	17,4	9,4	2,7
	ADTH 11	42	26,2	15,1	8,1	4,5	1,5
	ADTH 21	64,9	35,4	22,9	13,1	7,2	2,7
	ADTH 35	39,2	25,8	15	8,4	2,5	0,8
	ADTH 42	81,1	44,2	24,7	15,7	7,7	2,8
	ADTH 43	58,5	40,1	26,8	17,5	8,7	2,3
Cubilia bedding mortars	ADTH 23	45	23	8,7	5,6	3,2	1,4
	ADTH 46	24	14,1	9,9	6,1	2,7	1
	ADTH 54	73,9	53,2	32,8	14,3	6,7	2,6
Floor-coating bedding mortars	ADTH 24	66,4	49,7	36	22,6	12,6	4,2
	ADTH 28	88,5	67,7	50,9	35,2	19,2	4,1
	ADTH 34	69,9	42,9	26,8	15,7	6,2	1,9
	ADTH 37	94,1	59,1	35,7	19,6	10	3,8
Wall-coating bedding mortars	ADTH 7	39,9	28,1	18	10,4	5	1,5
	ADTH 31	72,0	48,1	26,8	15,3	7,5	2,9
	ADTH 52	68,4	38,2	21,9	12,1	6,4	2,5
Floor conglomerates *(rudus)*	ADTH 3	29,5	15,9	9,4	5,6	3	1,3
	ADTH 15	37,5	23,1	11,6	5,7	3,1	1,1
	ADTH 25	43,4	28,2	15,8	6,9	3,9	1,3
	ADTH 32	34,6	22,3	15,8	10,6	5,7	2,4
	ADTH 33	42,6	29,5	19,2	11,2	7,0	3,1
Wall conglomerates *(trullisatio)*	ADTH 18	61,7	42,1	28,3	20	11	4,2
	ADTH 26	65,8	42,3	26,7	15,5	7,6	2,8
	ADTH 58	40,8	26,2	16,6	9,8	4,7	1,6
Vaults concretes	ADTH 12	76,9	43	27	16,2	8,3	3,2
	ADTH 50	77,1	46,8	30	19,8	10,4	3,1
	ADTH 53	67,8	44,3	29,8	17,6	9,3	3,3
Plasters	ADTH 13	41,4	19,1	10	5,5	2,1	0,8
	ADTH 14	31,8	20,9	14,7	9,5	4,7	1,5

Table 10

Mortar typology	Sample	ρ_R	ρ_B	$\Phi_O He$	$\Phi_O H_2O$	CI_W	SI	Is_{50}
		(g/cm^3)	(g/cm^3)	(%)	(%)	(%)	(%)	(MPa)
Brick bedding mortars	ADTH 4	2.66	1.36	48.82	42.91	31.32	87.90	0.35
	ADTH 6	2.65	1.42	46.21	38.33	26.80	82.95	0.11
	ADTH 11	2.71	1.49	45.13	41.73	27.94	92.46	0.14
	ADTH 21	2.40	1.35	43.82	40.12	28.49	91.55	0.15
	ADTH 35	2.43	1.51	37.70	37.00	24.36	98.15	0.25
	ADTH 42	2.61	1.57	39.83	35.65	22.61	89.51	0.55
	ADTH 43	2.48	1.49	39.96	37.65	25.19	94.21	0.28
	Mean	2.56	1.46	43.07	39.06	26.67	90.96	0.26
	S.D.	0.12	0.08	4.01	2.63	2.90	4.84	0.15
Cubilia bedding mortars	ADTH 23	2.69	1.36	49.59	41.86	30.63	84.41	0.37
	ADTH 46	2.70	1.51	44.12	36.79	24.20	83.37	0.32
	ADTH 54	2.50	1.47	41.02	39.53	26.56	96.35	0.77
	Mean	2.63	1.45	44.91	39.39	27.13	88.05	0.49
	S.D.	0.11	0.08	4.34	2.54	3.25	7.21	0.24
Floor-coating bedding mortars	ADTH 24	2.52	1.38	45.30	43.80	31.44	96.70	0.18
	ADTH 28	2.75	1.57	43.23	37.19	23.63	86.03	0.11
	ADTH 34	2.60	1.27	51.19	47.01	36.68	91.83	0.37
	ADTH 37	2.51	1.39	44.72	41.17	29.50	92.06	0.45
	Mean	2.60	1.40	46.11	42.29	30.31	91.66	0.28
	S.D.	0.11	0.12	3.50	4.16	5.39	4.37	0.16
Wall-coating bedding mortars	ADTH 7	2.64	1.40	47.17	37.53	26.71	79.56	0.08
	ADTH 31	2.68	1.49	44.48	37.41	25.04	84.12	0.37
	ADTH 52	2.61	1.25	51.98	45.56	35.99	87.64	0.31
	Mean	2.64	1.38	47.88	40.17	29.24	83.77	0.25
	S.D.	0.03	0.12	3.80	4.67	5.90	4.05	0.15
Floor conglomerates *(rudus)*	ADTH 3	2.67	1.56	41.37	40.14	25.48	97.04	0.95
	ADTH 15	2.59	1.49	42.70	36.73	24.63	86.02	0.47
	ADTH 25	2.48	1.40	43.57	39.56	26.96	90.78	0.57
	ADTH 32	2.54	1.47	41.99	36.72	24.80	87.44	0.41
	ADTH 33	2.65	1.57	40.98	36.36	23.11	88.73	0.26
	Mean	2.59	1.50	42.12	37.90	25.00	90.00	0.53
	S.D.	0.08	0.07	1.04	1.80	1.40	4.31	0.26
Wall conglomerates *(trullisatio)*	ADTH 18	2.62	1.35	48.43	39.06	28.66	80.64	0.11
	ADTH 26	2.25	1.21	46.38	44.94	36.96	96.89	0.47
	ADTH 58	2.21	1.46	34.14	32.81	22.31	96.08	0.57
	Mean	2.36	1.34	42.99	38.93	29.31	91.20	0.38
	S.D.	0.23	0.13	7.72	6.07	7.35	9.15	0.24
Vault concretes	ADTH 12	2.56	1.46	42.79	37.80	25.65	88.33	0.25
	ADTH 50	2.66	1.36	49.02	44.55	32.58	90.88	0.23
	ADTH 53	2.63	1.37	47.83	42.07	30.35	87.93	0.33
	Mean	2.62	1.40	46.55	41.47	29.53	89.05	0.27
	S.D.	0.05	0.06	3.30	3.41	3.54	1.60	0.05
Plasters (*arriccio*)	ADTH 13	2.44	1.55	36.64	36.19	23.28	98.79	0.64
	ADTH 14	2.54	1.53	39.64	37.82	24.59	95.40	0.71
	Mean	2.49	1.54	38.14	37.01	23.94	97.09	0.68
	S.D.	0.07	0.01	2.13	1.15	0.92	2.40	0.05

Table 11

Binder and aggregate typology	Sample	ρ_R	ρ_B	$\Phi_O He$	$\Phi_C He$	Φ_T	$\Phi_O H_2O$	CI_W	SI
		(g/cm^3)	(g/cm^3)	(%)	(%)	(%)	(%)	(%)	(%)
Brick bedding mortar binders	ADTH 4	1,67	0,58	39,61	13,88	53,49	31,52	26,39	79,57
	ADTH 6	1,52	0,60	33,17	18,19	51,35	22,37	17,94	67,44
	ADTH 11	2,67	1,28	49,49	2,16	51,65	44,20	30,86	89,31
	ADTH 21	1,53	0,71	36,57	21,00	57,58	31,55	25,08	86,25
	ADTH 35	0,81	0,48	15,77	41,53	57,30	16,08	11,50	101,94
	ADTH 42	2,57	1,47	41,43	4,74	46,17	34,46	21,81	83,17
	ADTH 43	1,59	0,90	28,99	24,39	53,38	26,38	18,83	91,00
	Mean	1,77	0,86	35,00	17,99	52,99	29,51	21,77	85,53
	S.D.	0,65	0,38	10,68	13,21	3,90	9,03	6,37	10,66
Cubilia bedding mortar binders	ADTH 23	1,90	0,66	44,02	11,20	55,23	32,53	27,26	73,90
	ADTH 46	2,13	1,01	39,32	11,35	50,67	27,85	19,13	70,84
	ADTH 54	1,18	0,58	24,58	28,64	53,23	23,60	17,19	95,99
	Mean	1,74	0,75	35,97	17,07	53,04	28,00	21,19	80,24
	S.D.	0,50	0,23	10,14	10,03	2,28	4,47	5,34	13,72
Floor-coating bedding mortar binders	ADTH 24	1,44	0,59	34,25	19,95	54,20	33,24	26,80	97,07
	ADTH 28	1,42	0,60	27,40	20,79	48,19	20,01	12,73	73,05
	ADTH 34	1,47	0,38	41,37	12,17	53,54	36,32	33,53	87,78
	ADTH 37	2,43	1,16	51,14	6,32	57,46	45,48	35,48	88,95
	Mean	1,69	0,68	38,54	14,81	53,35	33,77	27,13	86,71
	S.D.	0,49	0,34	10,15	6,86	3,84	10,54	10,30	10,00
Wall-coating bedding mortar binders	ADTH 7	1,90	0,74	42,37	12,62	54,98	27,38	22,16	64,61
	ADTH 31	2,36	1,13	44,19	7,50	51,69	32,50	22,96	73,54
	ADTH 52	1,76	0,48	48,10	10,12	58,22	38,76	36,16	80,59
	Mean	2,01	0,78	44,89	10,08	54,97	32,88	27,09	72,91
	S.D.	0,31	0,33	2,93	2,56	3,26	5,70	7,86	8,01
Floor conglomerate *(rudus)* binders	ADTH 3	1,49	0,77	25,88	23,93	49,81	25,66	16,26	99,13
	ADTH 15	1,90	0,95	36,03	16,19	52,22	27,42	19,63	76,11
	ADTH 25	1,23	0,50	30,86	22,69	53,55	26,43	19,71	85,64
	ADTH 32	1,53	0,74	31,34	22,20	53,53	24,65	18,24	78,66
	ADTH 33	1,71	0,89	30,06	20,12	50,18	24,32	15,56	80,90
	Mean	1,57	0,77	30,83	21,03	51,86	25,69	17,88	84,09
	S.D.	0,25	0,17	3,62	3,03	1,79	1,27	1,91	9,11
Wall conglomerate *tTrullisatio)* binders	ADTH 18	1,83	0,60	46,09	11,53	57,62	32,23	27,23	69,92
	ADTH 26	1,64	0,63	50,31	15,79	66,10	49,47	47,19	98,34
	ADTH 58	0,92	0,68	16,63	49,72	66,35	16,19	12,62	97,33
	Mean	1,46	0,64	37,68	25,68	63,36	32,63	29,01	88,53
	S.D.	0,48	0,04	18,35	20,92	4,97	16,65	17,35	16,12
Vault concrete binders	ADTH 12	1,54	0,75	30,80	21,87	52,67	24,09	17,90	78,22
	ADTH 50	1,38	0,41	35,04	14,93	49,97	29,68	25,12	84,69
	ADTH 53	1,58	0,57	37,08	15,77	52,86	29,32	24,24	79,07
	Mean	1,50	0,57	34,31	17,52	51,83	27,70	22,42	80,66
	S.D.	0,10	0,17	3,21	3,79	1,62	3,13	3,94	3,52
Plasters (*arriccio*) binders	ADTH 13	2,58	1,61	41,49	5,00	46,49	42,08	27,53	101,40
	ADTH 14	1,58	0,87	28,60	23,90	52,49	27,31	18,28	95,50
	Mean	2,08	1,24	35,05	14,45	49,49	34,69	22,91	98,45
	S.D.	0,70	0,52	9,12	13,36	4,24	10,44	6,55	4,17
Volcanic scoria aggregates	ADTH 33 b	2,40	1,46	39,28	n.d.	n.d.	38,01	26,07	96,90
	ADTH 18 b	2,53	1,53	39,74	n.d.	n.d.	39,07	25,63	98,44
	ADTH 50 b	2,56	1,57	38,54	n.d.	n.d.	37,93	24,18	98,55
	ADTH 11 b	2,58	1,67	35,42	n.d.	n.d.	35,20	21,13	99,55
	ADTH 34 b	2,56	1,63	36,27	n.d.	n.d.	36,15	22,16	99,81
	ADTH 14 b	2,53	1,61	36,26	n.d.	n.d.	36,21	22,47	100,01
	ADTH 12 b	2,51	1,55	38,21	n.d.	n.d.	32,46	20,69	84,96
	Mean	2,53	1,57	37,67	n.d.	n.d.	36,43	23,19	96,89
	S.D.	0,06	0,07	1,68	n.d.	n.d.	2,20	2,13	5,37
Leucitite aggregates	ADTH 35 l	2,87	2,16	24,68	n.d.	n.d.	23,66	10,94	95,89
	ADTH 58 l	2,88	2,06	28,52	n.d.	n.d.	26,11	12,66	91,57
	ADTH 25 l	2,87	2,18	25,68	n.d.	n.d.	20,87	9,56	87,48
	Mean	2,87	2,13	26,29	n.d.	n.d.	23,55	11,05	91,65
	S.D.	0,01	0,06	1,99	n.d.	n.d.	2,62	1,55	4,21
Cocciopesto aggregates	ADTH 18 c	2,85	1,58	44,49	n.d.	n.d.	38,39	24,11	86,30
	ADTH 25 c	2,30	1,92	16,61	n.d.	n.d.	12,27	7,49	73,86
	ADTH 3 c	2,92	1,52	47,97	n.d.	n.d.	42,52	27,82	88,65
	ADTH 11 c	1,95	1,68	13,67	n.d.	n.d.	13,44	7,02	98,29
	Mean	2,51	1,68	30,68	n.d.	n.d.	26,65	16,61	86,78
	S.D.	0,46	0,17	18,04	n.d.	n.d.	16,03	10,91	10,05

Table 12

Mortar tipology	Samples	Water absorption (%)									
		24 h	48 h	72 h	96 h	120 h	144 h	168 h	192 h	216 h	240 h
Briks bedding mortars	ADTH 4	28.53	29.44	29.91	30.53	30.86	30.94	31.10	31.28	31.31	31.32
	ADTH 6	23.16	24.20	24.99	25.44	25.94	26.11	26.26	26.46	26.69	26.80
	ADTH 11	24.97	25.53	26.03	26.74	27.24	27.33	27.55	27.49	27.95	27.94
	ADTH 21	25.44	25.87	26.30	26.71	27.00	27.32	27.62	27.92	28.49	28.49
	ADTH 35	22.79	23.26	23.34	23.88	24.25	24.29	24.15	24.07	24.36	24.36
	ADTH 42	19.53	20.38	21.21	21.77	22.03	22.46	22.61	22.35	22.61	22.61
	ADTH 43	22.17	23.03	23.39	24.21	24.15	24.47	24.84	24.77	25.19	25.19
Cubilia bedding mortars	ADTH 23	27.86	27.95	28.08	28.78	29.14	29.70	29.96	30.03	30.35	30.63
	ADTH 46	21.86	22.40	22.59	22.86	23.04	23.18	23.31	23.68	24.20	24.20
	ADTH 54	24.45	23.70	23.92	25.22	25.41	25.00	25.44	25.64	26.56	26.56
Floor-coating bedding mortars	ADTH 24	27.43	27.95	28.32	29.01	29.55	30.24	30.57	30.75	31.44	31.44
	ADTH 28	21.44	21.97	22.13	22.35	22.46	22.75	22.95	23.11	23.63	23.63
	ADTH 34	32.28	32.89	33.61	33.78	34.39	34.65	35.08	35.54	36.68	36.68
	ADTH 37	26.75	27.14	27.67	28.27	28.38	28.50	28.54	28.52	29.50	29.50
Wall-coating bedding mortars	ADTH 7	24.93	24.97	25.09	25.41	25.73	25.91	26.31	26.51	26.71	26.71
	ADTH 31	23.83	23.99	24.06	24.25	24.46	24.65	24.86	24.95	25.02	25.04
	ADTH 52	31.49	33.03	33.39	33.87	34.45	34.58	34.69	35.04	35.99	35.99
Floor conglomerates *(rudus)*	ADTH 3	22.78	23.67	24.16	24.31	24.47	24.87	25.05	24.88	25.48	25.48
	ADTH 15	23.40	23.47	23.51	23.71	23.90	24.10	23.31	24.51	24.63	24.63
	ADTH 25	24.14	25.21	26.23	26.53	26.72	26.86	26.93	26.96	26.96	26.96
	ADTH 32	20.33	21.04	22.20	23.19	23.32	23.69	23.98	24.34	24.80	24.80
	ADTH 33	19.24	19.93	20.09	21.05	21.51	21.95	22.23	22.60	23.11	23.11
Wall conglomerates *(trullisatio)*	ADTH 18	24.35	26.37	26.56	27.33	27.44	27.76	27.80	28.05	28.66	28.66
	ADTH 26	34.47	35.18	35.38	35.32	35.59	35.63	35.96	36.08	36.96	36.96
	ADTH 58	20.66	20.48	20.69	21.20	21.14	21.60	21.66	21.52	22.31	22.31
Vaults concretes	ADTH 12	22.73	23.22	23.76	24.20	24.20	24.75	25.23	25.01	25.65	25.65
	ADTH 50	28.37	29.18	29.98	30.98	31.83	31.67	31.70	31.91	32.58	32.58
	ADTH 53	26.21	26.69	27.16	27.94	28.41	28.77	29.32	29.81	30.35	30.35
Plasters	ADTH 13	21.19	21.75	22.17	22.38	22.64	22.71	22.83	22.92	23.29	23.28
	ADTH 14	22.15	22.79	23.17	23.83	24.00	24.03	24.08	24.14	24.59	24.59

Table 13

Mortar	Samples	D (mm)	W (mm)	2L (mm)	P(N)	A=WD (mm^2)	De^2(mm^2)	De (mm)	$Is_{(50)}$ (Mpa)	R_c (Mpa)	R_T (Mpa)
Brick bedding mortars	ADTH 4	13.50	16.50	10.6	160	222.75	283.62	16.84	0.35	4.84	0.43
	ADTH 6	14.00	16.00	11	50	224.00	285.21	16.89	0.11	1.51	0.13
	ADTH 11	14.00	15.00	10.25	60	210.00	267.39	16.35	0.14	1.90	0.17
	ADTH 21	9.20	15.50	10.5	50	142.60	181.57	13.47	0.15	2.14	0.19
	ADTH 35	14.10	16.90	10.5	120	238.29	303.41	17.42	0.25	3.45	0.31
	ADTH 42	15.30	16.50	10.75	280	252.45	321.44	17.93	0.55	7.69	0.69
	ADTH 43	16.10	17.10	10.35	150	275.31	350.55	18.72	0.28	3.85	0.34
Cubilia bedding mortars	ADTH 23	13.40	14.00	10.5	310	187.60	238.87	15.46	0.77	10.71	0.96
	ADTH 46	13.80	16.10	11.5	150	222.18	282.90	16.82	0.32	4.55	0.41
	ADTH 54	14.30	14.30	9.55	160	204.49	260.37	16.14	0.37	5.17	0.46
Floor-coating bedding mortars	ADTH 24	12.00	17.40	10.5	80	208.80	265.86	16.31	0.18	2.54	0.23
	ADTH 28	15.90	16.50	10.45	60	262.35	334.04	18.28	0.11	1.60	0.14
	ADTH 34	12.80	16.20	10.75	160	207.36	264.03	16.25	0.37	5.12	0.46
	ADTH 37	14.10	16.10	9.5	210	227.01	289.05	17.00	0.45	6.26	0.56
Wall-coating mortars	ADTH 7	15.00	15.50	10.25	40	232.50	296.04	17.21	0.08	1.17	0.10
	ADTH 31	13.40	14.00	10.5	150	187.60	238.87	15.46	0.37	5.18	0.46
	ADTH 52	13.50	16.00	11.15	140	216.00	275.03	16.58	0.31	4.34	0.39
Floor conglomer. *(rudus)*	ADTH 3	14.00	15.90	9.5	440	222.60	283.43	16.84	0.95	13.32	1.19
	ADTH 15	13.80	16.20	10.05	220	223.56	284.65	16.87	0.47	6.64	0.59
	ADTH 25	12.50	17.50	10.75	260	218.75	278.53	16.69	0.57	7.98	0.71
	ADTH 32	14.90	15.00	10.5	190	223.50	284.58	16.87	0.41	5.73	0.51
	ADTH 33	15.50	11.60	10.4	100	179.80	228.94	15.13	0.26	3.57	0.32
Wall conglomer *(trullisatio).*	ADTH 18	14.10	16.20	9.75	50	228.42	290.84	17.05	0.11	1.48	0.13
	ADTH 58	14.10	16.10	10.95	220	227.01	289.05	17.00	0.47	6.56	0.59
	ADTH 26	14.40	17.50	10.5	290	252.00	320.87	17.91	0.57	7.97	0.71
Vault concretes	ADTH 12	13.40	15.80	9.5	110	211.72	269.58	16.42	0.25	3.46	0.31
	ADTH 50	12.00	17.20	10.5	100	206.40	262.80	16.21	0.23	3.21	0.29
	ADTH 53	13.90	15.70	10.45	150	218.23	277.87	16.67	0.33	4.61	0.41
Plasters	ADTH 13	16.50	16.70	13	350	275.55	350.85	18.73	0.64	8.98	0.80
	ADTH 14	16.20	17.10	10	390	277.02	352.72	18.78	0.71	9.96	0.89